CHAPTER FIVE

Effects of mantle dynamics

Summary

Plate tectonics operates in the upper thermal boundary layer of an underlying mantle convection system. Flow within the mantle takes place at different spatial scales, including flows induced by the subduction of cold lithospheric slabs, incubation under continental lids, small-scale convection driven by edge effects, lower-mantle megaplumes, and upper-mantle hotspots. This flow and the consequent mass anomalies at depth result in a dynamic topography at the Earth's surface that is important in basin analysis.

The starting point for an analysis of mantle flow is a consideration of buoyancy forces set up by density heterogeneities in the mantle. Buoyancy forces are counteracted by viscous resistance. The force balance provides fundamental information about the scaling between parameters and allows the derivation of dimensionless groups that describe various aspects of the flow and thermal characteristics of a fluid layer, such as the Rayleigh number. Consideration of the Rayleigh number for the mantle indicates that convection must be occurring. This convective flow efficiently transports heat and drives high plate velocities, but is laminar.

Numerical and physical experiments illustrate the convection patterns of upwellings and downwellings produced by heating a fluid layer from below, from the surface and with internal radiogenic heating. Models using highly temperature-dependent viscosity structures in the mantle suggest that large aspect ratio convection cells are stable, such as must underlie the Pacific plate. Detailed three-dimensional velocity models of the mantle (seismic tomography) also show mass anomalies that must be sustained by flow. These mass anomalies show that the effects of plate tectonics, such as mid-ocean ridges and subducting slabs, can be recognised deep into the Earth's interior.

Measurements of the Earth's gravity field reveal geoid height anomalies. An underlying convecting system should produce variations in the height of the geoid over upwelling and downwelling limbs. At long wavelength, the observed geoid of the Earth shows major zones of positive and negative geoid anomaly. Viscous flow models of the mantle suggest that mass excesses in the upper mantle caused by the remnants of cold subducted slabs generate geoid lows, whereas hotspots and mid-ocean ridges are correlated with the presence of hot megaplumes in the lower mantle and are associated with geoid highs.

The surface topography on land, and the bathymetry beneath the sea, produced by mantle flow, is known as dynamic topography. It represents a deflection of the surface of the Earth caused by the presence of 'blobs' of buoyancy in the mantle. It can be recognised, for example, in regions of plate subduction due to the cooling effect of the oceanic slab, beneath supercontinents due to heating caused by the presence of an insulating lid, near the edges of continents due to small-scale convection triggered by the ocean–continent boundary, and, of course, in the form of topographic 'hotspot' swells in the ocean associated with magmatism. Some of the sub-plate flow structures responsible for topographic doming and magmatism are thought to be plumes originating from the core–mantle boundary. There is evidence of unsteadiness in plume activity, with pulses of buoyancy causing relatively rapid uplift of the Earth's surface followed by subsidence. Such pulses may cause cycles of erosional landscape development and delivery of sands to the deep sea, followed by draping with marine sediments.

Mantle flow is commonly associated with melt generation, igneous underplating and surface magmatism. The presence of plumes may cause sufficient elevation of asthenospheric temperatures to result in adiabatic decompression and the formation of flood basalt provinces (large igneous provinces – LIPs). The North Atlantic igneous province and the Ethiopian Afar regions are examples. LIPs are commonly connected to currently active volcanic hotspots by tracks of extinct volcanoes.

Mantle dynamics affects basin development by causing topographic uplift and the export of particulate sediment from erosional landscapes to sedimentary basins. Mantle dynamics also causes negative dynamic topography in the form of sag-type basins of the continental interiors. In geological history, cratonic basins have initiated preferentially at times of continental dispersal away from supercontinental assemblies. Their long, slow subsidence has been attributed to negative dynamic topography over cold downwellings, to thermal contraction of previously stretched and heated thick continental lithosphere, and to sediment loading following an earlier stage of stretching.

Dynamic uplift of the continental surface produces domal features that promote centrifugal river drainage patterns. The periods of dynamic uplift can potentially be recognised by the location of erosive knickzones in the river long profile. Time-varying dynamic topography may also affect the position of continental drainage divides and the direction of river discharge to the ocean, as in the reversal of Amazon drainage from the Pacific to the Atlantic.

Dynamic topography is also a primary factor in the history of long-term sea-level change and the extent of continental flooding. In particular, times of extensive uplift of the seafloor in the form of superswells, as in the Pacific during the Cretaceous, may be primarily responsible for elevated sea levels, rather than reflecting increases in spreading rate in the mid-ocean ridge system.

Basin Analysis: Principles and Application to Petroleum Play Assessment, Third Edition. Philip A. Allen and John R. Allen.

5.1 Fundamentals and observations

5.1.1 Introduction: mantle dynamics and plate tectonics

Although plate tectonics has been highly successful as an explanation of the relative motion of plates and the deformation at their boundaries, there is little integration of mantle dynamics into what is essentially a kinematic theory. For example, volcanic hotspots such as those of Hawaii and Iceland, which are related to the ascent of deeply rooted mantle plumes, do not fit into plate tectonic theory. Within the solar system, the operation of plate tectonics is unique to Earth, but plume volcanism occurs on Mars and Venus as well as on a number of moons. The surface of Mars appears to be a single static plate acting as a 'frozen lid'; Venus is a convecting planet beneath a thick viscous lid, but no mobile plates, and the tectonics is spatially continuous and unstable. On Earth, therefore, we have a particular problem in understanding the interaction of internal thermal convection with an upper thermal boundary layer made of a discrete number of plates in relative motion.

The three-dimensional mapping of seismic velocity variations in the mantle (seismic tomography) now provides unprecedented detail on small but systematic density variations that reflect temperature (and/or chemical) heterogeneities. These heterogeneities reveal a picture of deep penetration of cold subducted lithospheric slabs into the mantle, and of large hot upwellings that seem to rise from a highly dynamic core–mantle boundary (Fig. 5.1). Subducted slabs of lithosphere appear to both penetrate and to queue at the 670 km discontinuity. The residues of the subducted slabs that penetrate the discontinuity appear to descend to the core–mantle boundary, where they are reheated before being resurrected as a mantle plume. Mantle plumes appear to travel upwards and impinge on the base of the lithosphere, spreading out like a mushroom, and uplifting the overlying plate. Extension of the lithosphere over the plume head may lead to continental splitting (Chapter 3), the formation of new spreading centres and further subduction of lithosphere.

Convection systems in the mantle are the engines for the surface tangential motions of plates. Subducting slabs are cold downwellings, and spreading oceanic ridges are upwellings (Davies & Richards 1992), so the lithospheric plates must be regarded as an integral part of the convection system rather than being dragged passively by basal traction over the convection system. In other words, plate tectonics is the surface expression of convection.

Plate tectonic theory explains a wide range of geological and geophysical observations in the oceans and at plate boundaries. It has been far less successful in explaining the topography, seismicity, neo-

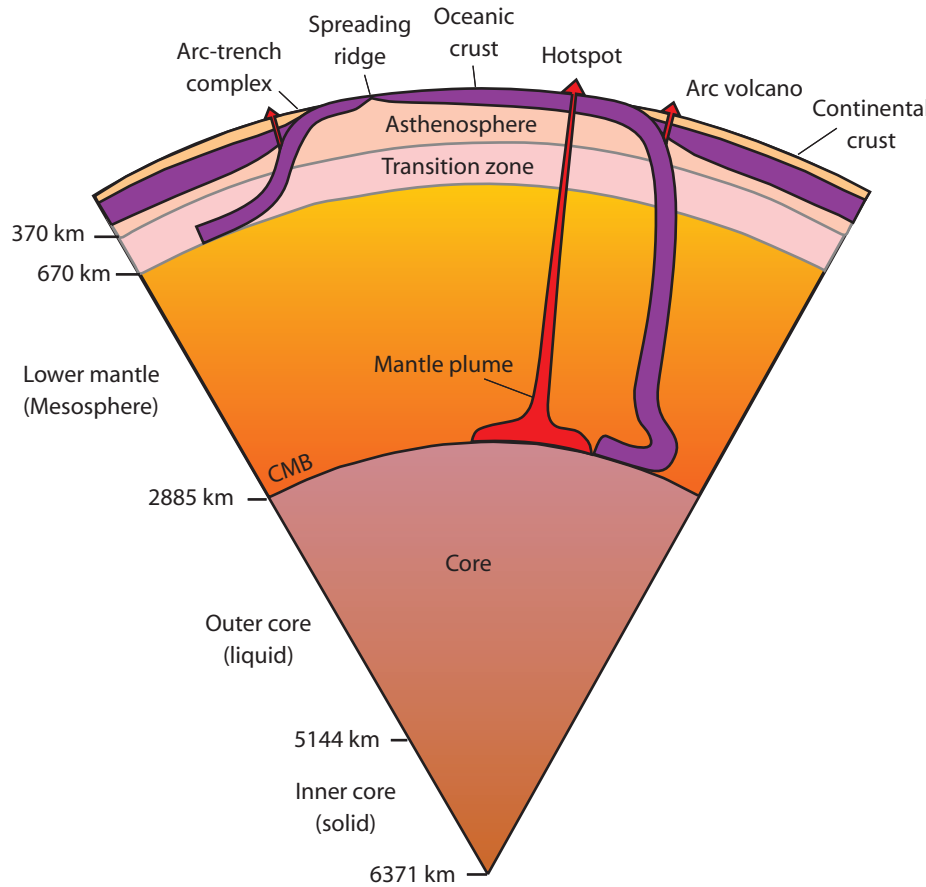

Fig. 5.1 Schematic section through a segment of the Earth showing the subduction of lithospheric slabs that are laid out along the 670 km discontinuity or penetrate to a graveyard above the core–mantle boundary (CMB). A mantle plume is shown rising from the CMB to produce a hotspot in the overlying oceanic plate. Modified from Stern (2002) and reproduced with permission of John Wiley & Sons, Inc.

tectonics and subsidence history of the continental interiors. This is partly due to the complex rheology of the continental lithosphere, and partly due to the lack of integration of mantle dynamics into a satisfactory explanation of continental deformation and basin development. Stratigraphers have long recognised the supreme importance of vertical movements ('epeirogeny') of the continents in generating the stratigraphic sequences of the world's cratons (Sloss 1963). In particular, the major transgressions of the continents that have taken place through geological time (e.g. Cambrian–Early Ordovician and Late Cretaceous, Bond 1979) cannot be explained purely by a eustatic sea-level rise (Bond 1976, 1978) and must involve a major component of widespread relative sea-level rise most likely related to mantle processes (§5.4.3).

It is increasingly recognised, therefore, that the near-surface motion of lithospheric plates needs to be understood by reference to the mantle convection system (Anderson 1982). In Chapter 5, we look briefly at the evidence for flow in the mantle, with the specific goal of understanding the significance of this flow for subsidence within continental sedimentary basins. The reader is referred to §2.2.8 for introductory material on mantle viscosity, convection in the mantle and the adiabatic temperature gradient. The rheology of mantle rocks is dealt with in §2.3.2.

5.1.2 Buoyancy and scaling relationships: introductory theory

The buoyancy contrasts of the interior of the Earth, which are the forces responsible for its flow, derive essentially from lateral (horizontal) density contrasts. These density contrasts may be thermal or compositional in origin.

Buoyancy results from gravity acting on a density contrast $\Delta\rho$ in a volume V. It is a force B given by

$$B = -gV\Delta\rho = -g\Delta m \qquad [5.1]$$

where Δm is the mass anomaly resulting from the density contrast and the minus sign is because gravity and weight are positive downwards whereas buoyancy is conventionally positive upwards (Davies 1999, p. 212). Consequently, the buoyancy force depends strongly on the volume of the density contrast. The density contrast resulting from temperature differences is given by the volumetric coefficient of thermal expansion α_v (eqn. [2.12]). Using parameter values for mantle rock, a temperature difference of 1000 °C causes just a 3% change in density. Nevertheless, large buoyancy forces in the mantle may result from the subduction of cold slabs of lithosphere (negative buoyancy) or from the presence of plume heads (positive buoyancy).

A simple consideration of the buoyancy forces associated with the motion of plates explains convection in the mantle (Turcotte & Oxburgh 1967) (see §5.1.3). A plate represents a cooled thermal boundary layer, so is cold and tends to sink due to negative buoyancy. The sinking is opposed by viscous stresses caused by the resulting flow of the mantle, with the stresses increasing with the velocity of the sinking. Consequently, a balance is reached between the viscous resistance and the negative buoyancy at a certain velocity u, given by Davies (1999, p. 216)

$$u = D\left(\frac{g\rho\alpha_v T\sqrt{\kappa}}{4\mu}\right)^{2/3} \qquad [5.2]$$

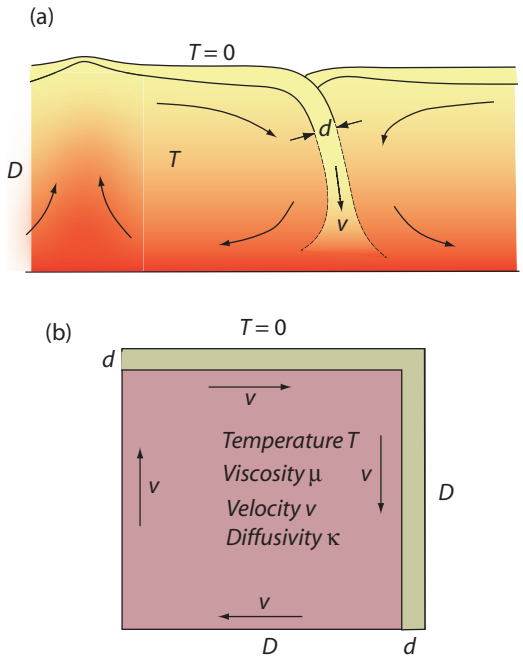

Fig. 5.2 Sketch (a) and model set-up (b) of a convective flow driven by subduction at velocity v of a plate thickness d in a fluid layer of thickness D, viscosity μ and temperature T. After Davies (1999, p. 214), © Cambridge University Press, 1999.

where D is the depth of the vertically descending slab, and ρ, μ, κ and T are the density, viscosity, thermal diffusivity and temperature of the interior of the fluid mantle (Fig. 5.2). Using parameter values of $D = 3000$ km (thickness of the whole mantle), $\rho = 4000\,\mathrm{kg\,m^{-3}}$, $T = 1400$ °C, $\mu = 10^{22}$ Pa s, $\alpha = 2 \times 10^{-5}\,^{\circ}\mathrm{C}^{-1}$ and $\kappa = 10^{-6}\,\mathrm{m^2\,s^{-1}}$, the downward velocity is $90\,\mathrm{mm\,yr^{-1}}$. This is close to the known velocities of plate motion (Lithgow-Bertelloni & Richards 1998).

The same force balance allows the thickness of the lithosphere at the point of subduction d to be estimated, treating it as a diffusive length scale (see §2.2.7) equal to $\sqrt{\kappa t}$ (or $\sqrt{\kappa D/u}$), and the surface heat flux to be estimated, using Fourier's law (see §2.2.2), which states $q = KT/d$ where K is the thermal conductivity. Using the same parameter values as above, and $K = 3\,\mathrm{W\,m^{-1}\,K^{-1}}$, we obtain 33 km for the thickness of the oceanic lithosphere and $130\,\mathrm{mW\,m^{-2}}$ for the surface oceanic heat flow. These values are consistent with observations of oceanic plates, suggesting that a basic theory of mantle flow driven by buoyancy explains at first order the velocities of plates.

Combining eqn. [5.2] and the expression for diffusion length ($d = \sqrt{\kappa t}$) gives an expression with two dimensionless groups that embeds how the different parameters scale:

$$\left(\frac{D}{d}\right)^3 = \frac{g\rho\alpha T D^3}{4\kappa\mu} \qquad [5.3]$$

For example, eqn. [5.3] can be used to ask 'what would be the lithospheric thickness, heat flow and plate velocity if the mantle viscosity were 10 times lower at some early stage in the evolution of the Earth'? Keeping other parameter values constant, the plate thickness would reduce to 15 km, the heat flow would increase to $275\,\mathrm{mW\,m^{-2}}$, and the plate velocity would increase to c.$400\,\mathrm{mm\,yr^{-1}}$.

The right-hand side of eqn. [5.3] is a dimensionless group that contains a great deal of information about convection of a fluid layer. Removing the numerical factor 4, it is the *Rayleigh number*. The Rayleigh number is a measure of the likelihood and vigour of convection. For the parameter values above, the mantle has a **Ra** of c.3×10^6. Rewriting eqn. [5.3] it is clear that the length scale of the convection depends on the Rayleigh number **Ra** as follows

$$\frac{d}{D} = kRa^{-1/3} \qquad [5.4]$$

where the coefficient of proportionality k is about 1.6. In other words, if **Ra** increases, the cooled boundary layer of lithosphere d reduces in thickness relative to the depth of the convecting layer D. At $\mathbf{Ra} = 3 \times 10^6$, d is about 1% of the thickness of the convecting layer.

In a similar fashion, other parameter groups can be scaled against **Ra**. Instead of investigating length scales, we could choose velocities, in which case

$$\frac{u}{U} \sim Ra^{2/3} \qquad [5.5]$$

where U is the characteristic velocity of the problem equal to κ/D. This ratio u/U is a *Péclet number*, which for parameter values typical of the mantle is approximately 9000.

The heat flow q can also be expressed in terms of its scaling with the Rayleigh number. Modifying eqn. [5.4] with Fourier's law gives

$$q = \left(\frac{KT}{D}\right) Ra^{1/3} \qquad [5.6]$$

where the scaling variable (KT/D) expresses the heat that would be conducted across the entire fluid layer in the absence of convection. The total heat flow (in the presence of convection) q versus the conductive heat flow KT/D is known as the *Nusselt number*, **Nu**. Consequently, eqn. [5.6] becomes $\mathbf{Nu} \sim \mathbf{Ra}^{1/3}$. For the mantle, the Nusselt number is about 100, indicating that heat flow by convection is two orders of magnitude more efficient than that by conduction.

Accepting that the mantle is convecting in some way, it is possible to estimate whether the flow is laminar or turbulent. This is given by the Reynolds number **Re**

$$\mathrm{Re} = \frac{ud}{\nu} \qquad [5.7]$$

where u is the velocity of the flow, d is the length scale and ν is the kinematic viscosity equal to μ/ρ. The kinematic viscosity of the mantle is difficult to estimate, since it is dependent on the temperature, but let us take a value of $10^{17}\,\mathrm{m^2\,s^{-1}}$ as appropriate for the upper mantle. The flow velocity can be estimated from flow laws for incompressible Newtonian fluids; let us take $u\rho = 10^{-7}\,\mathrm{m\,s^{-1}}$ as an order of magnitude estimate ($1\,\mathrm{m\,yr^{-1}}$ is $3.17 \times 10^{-8}\,\mathrm{m\,s^{-1}}$, so u is about $30\,\mathrm{mm\,yr^{-1}}$ in this calculation). Using eqn. [5.7], **Re** is c.7×10^{-19}. This is much smaller than the critical **Re** for turbulence, indicating that the convecting flow in the mantle is laminar.

In summary, a simple quantitative model of convection involving a fluid layer with a cooled thermal boundary layer undergoing subduction allows the scaling relationships between parameter groups to be investigated. The Rayleigh number predicts the onset and vigour of convection, the Péclet number is a measure of the velocity of the plate as a cooled thermal boundary layer, the Nusselt number indicates the efficiency of heat flow by convection, and the Reynolds number is a measure of turbulence. For the mantle, $\mathbf{Ra} \approx 3 \times 10^6$, $\mathbf{Pe} \approx 9000$, $\mathbf{Nu} \approx 100$, and $\mathbf{Re} \approx 10^{-18}$, indicating a strongly convecting layer driving high plate velocities and vigorous heat loss, but laminar flow.

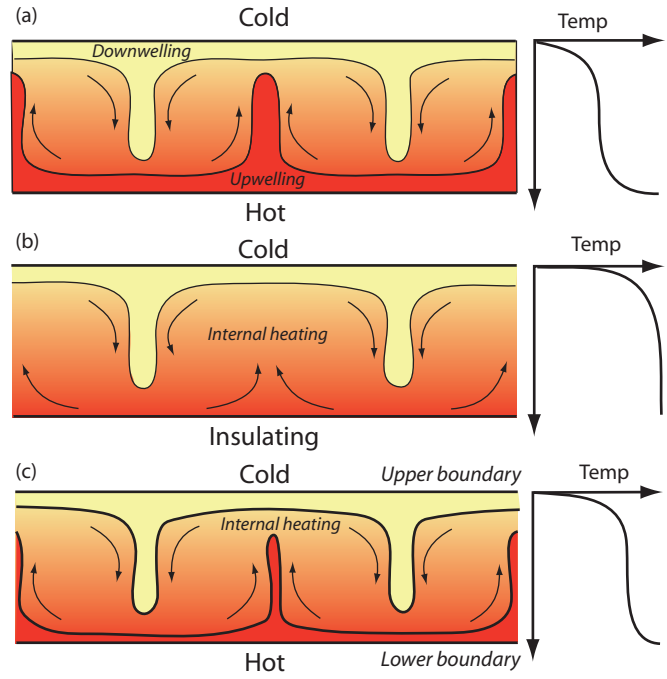

Fig. 5.3 Various modes of heating of a fluid layer, with temperature profiles. (a) Layer of fluid heated from below and cooled at the top. (b) Insulating (no flux) boundary below and internally self-heated by radiogenic decay. (c) Hot lower boundary and internally heated fluid layer. See text for explanation. After Davies (1999, p. 226) © Cambridge University Press, 1999.

5.1.3 Flow patterns in the mantle

The standard starting point for studies of convection is a layer of fluid heated from below and cooled at the top (Fig. 5.3a). Fluid close to the cold upper surface is cooled, forming a cold thermal boundary layer that is the lithosphere or plate. Likewise, fluid close to the hot lower surface is heated, forming a hot thermal boundary layer. Above a critical Rayleigh number, hot material rises from the lower boundary layer and reinforces the downward motion of fluid from the upper boundary layer, forming a series of rotating cells. The convection cells have a width that scales on the thickness of the fluid layer (Bercovici *et al.* 2000).

Differences in the flow patterns are expected depending on the precise conditions at the lower and upper boundaries and within the fluid layer itself. For example, if the fluid layer is self-heated by radiogenic heat production, and the lower boundary is insulating (involving no heat flow) (Fig. 5.3b), then cold downwellings would originate from the cooled upper boundary layer, but any upwellings would be a passive response rather than involving positively buoyant material. In other words, the fact that upwelling is occurring, as at mid-ocean ridges, does not mean that the ascending mantle material is hotter than average. The upwelling material is simply being displaced by the descending cold mantle material.

Perhaps the most characteristic feature of simple convection where a constant-viscosity layer is heated from below and cooled at the top is that it is symmetrical, consisting of sinking cold currents with an equal and opposite velocity and temperature to rising warm currents. In between the upper and lower thermal boundary layers, where temperature gradients are strong, is a well-mixed fluid at the average temperature of the bottom and top boundaries. The Earth's lithospheric plates comprise the upper thermal boundary layer. If the layer convects more vigorously (**Ra** increases), more of the layer will have a homogeneous temperature, the thermal boundary layers will be thinner and the temperature gradients through them will be higher, driving larger heat fluxes. Fluid in the gravitationally unstable thermal boundary layers must eventually either rise or sink, producing upwellings or downwellings, which therefore must set up a flow of material in the thermal boundary layer from divergent zones above upwellings to convergent zones at downwellings. The thermal boundary layers must thicken in the direction of motion. For example, hot fluid arriving above an upwelling zone travels towards a downwelling and cools to the surface as it does so, before becoming gravitationally unstable enough to sink. The simple theory of convection therefore explains many of the essential features of plate motion (§1.4).

The simplest type of convection is two-dimensional, with counter-rotating cylinders or rolls in the third dimension. The horizontal dimensions of the individual convecting cells in a fluid layer of vertical thickness D, heated from below, is approximately equal to D. This horizontal dimension is also the length of the horizontal currents in the thermal boundary layers. In the simplest terms, the length of the horizontal currents is determined by the amount of cooling necessary to induce gravitational instability and downwelling. At a higher Rayleigh number (**Ra** ~ 10^5) in fluids of constant viscosity, a three-dimensional pattern develops (Busse & Whitehead 1971), which may be bimodal or spoke-like, with linear upwellings joining at a vertex. Fluids with temperature-dependent viscosity produce three-dimensional polyhedral patterns of squares, triangles and hexagons.

The volume of mantle undergoing convection is a *spherical shell* whose outer surface area is over three times the area of the inner surface. This promotes a highly three-dimensional circulation and enhances the effects of layering in mantle viscosity. Spherical shell models (Bunge *et al.* 1996; Davies & Davies 2009) generate near-surface circulations that are very long in the horizontal dimension, with rising spoke-like columns and veins, and descending sheets (Fig. 5.4).

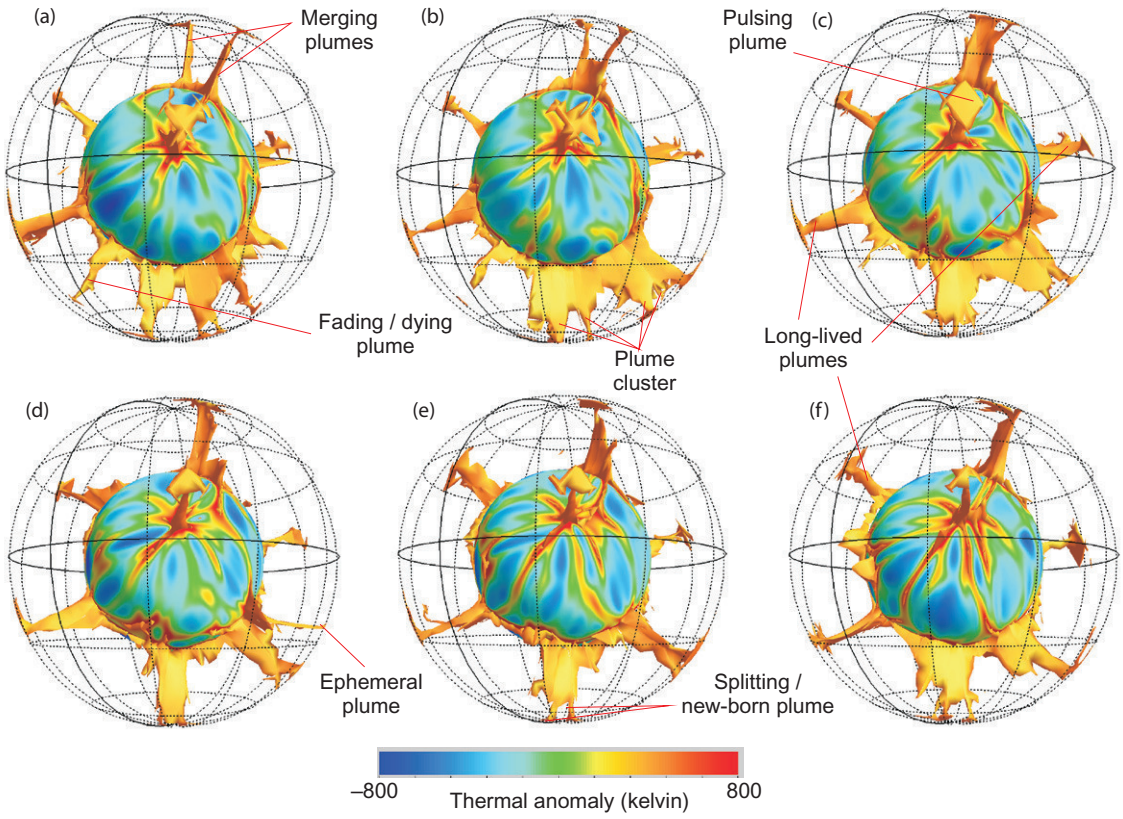

Fig. 5.4 Temporal evolution of an isochemical, incompressible mantle at a Rayleigh number of 1.4×10^9, forming a spherical shell, from Davies & Davies (2009). Each simulation, (a) to (f), is spaced 35 Myr apart. The temperature scale is the temperature in excess of or below the lateral average. Each snapshot shows a radial surface just above the core–mantle boundary and a hot iso-surface 500 K hotter than the average for their depth. Hot upwelling structures (plumes) are prominent. The majority are long-lived and migrate slowly, whereas others are more mobile and short-lived. Over time, new plumes form and old plumes fade and die. Smaller plumes may coalesce, and larger plumes may pulse in their intensity. Reprinted with permission from Elsevier.

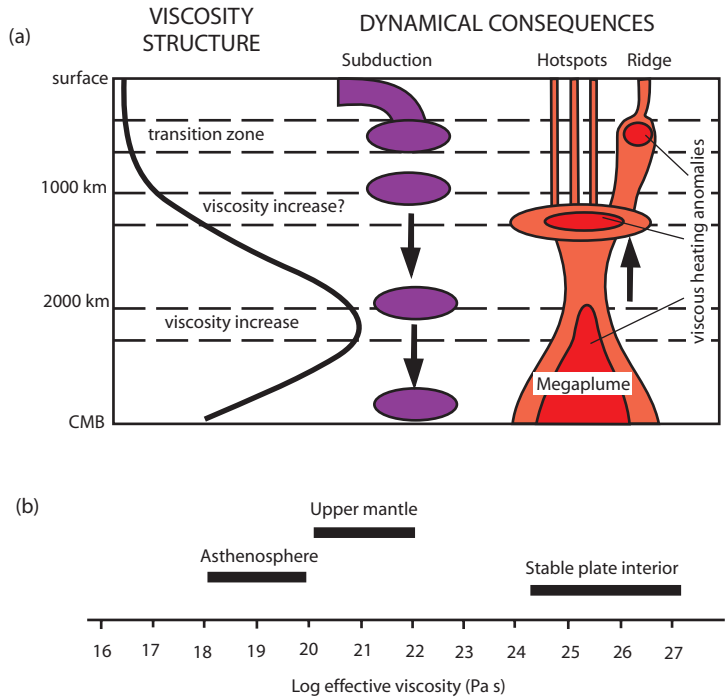

Fig. 5.5 (a) Schematic diagram showing the subduction of cold slabs and the development of megaplumes resulting in mid-ocean ridges and hotspots at the surface, based on seismic tomography of the mantle, adapted from Cadek *et al*. (1995) and reproduced with permission from Elsevier. CMB, core–mantle boundary. (b) Estimates of effective viscosities for stable plate interiors, upper mantle, and asthenosphere.

5.1.3.1 Effects of internal heating

We expect internal heating of the fluid layer to affect the spatial pattern of convection as well as the vigour. The simplest situation of internal heating would be a uniform distribution of heat production with depth, an isothermal upper boundary, and a zero heat flux through the insulating lower boundary (Fig. 5.3b). Because of the zero heat flux at the bottom boundary, no active upwellings occur, and instead a passive upward flow takes place to compensate for the active downwelling of cold material from the upper thermal boundary layer. If the bottom boundary is allowed to conduct a heat flux, and there is an internal heat generation (Fig. 5.3c), the upper boundary must conduct outwards both the basal heat as well as the internal heat. Consequently, the upper thermal boundary layer develops a greater temperature drop than the basal boundary. This causes the upper boundary to develop more numerous or more vigorous downwellings than upwellings rising from the lower boundary. Internal heating therefore breaks down the symmetry between upwellings and downwellings. Since the Earth is known to have very significant internal sources of heat relative to the basal heat flow from the core, we should expect downwellings of an upper thermal boundary layer to dominate the pattern of convection, and upwellings should be relatively weaker (Bercovici *et al*. 2000). This is precisely the situation seen at the Earth's surface.

5.1.3.2 Effects of a temperature-dependent viscosity

The viscosity of mantle materials obeys a temperature-dependent Arrhenius-type law (see also §10.2). Since the absolute temperature occurs in the denominator of the Arrhenius exponent, there are very large viscosity variations at lower temperatures. This is why the viscosity variation in the upper mantle may be extreme (Fig. 5.5a), from perhaps 10^{21} Pa s in its lower part to 10^{18} Pa s in the asthenosphere and 10^{25} Pa s in the lithosphere, representing a variation of viscosity of seven orders of magnitude in a depth range of just 200 km (Fig. 5.5b). This makes the lithosphere much stronger and potentially less mobile than the rest of the mantle. It in turn forces the underlying mantle to heat up, increasing the temperature contrast between the hot interior and the cold upper boundary. Since material in the upper thermal boundary layer must cool a great deal to become gravitationally unstable and sink relative to its cold, immobile surroundings, the horizontal extent of the convection cell may become elongated, as demonstrated in both laboratory and numerical experiments (Ratcliff *et al*. 1997). This would explain the very large lateral distance of the spreading ridge to the subducting margin of the Pacific plate. Large aspect ratio (long-wavelength) convection cells have also been imaged by seismic tomography (Su & Dziewonski 1992). With a stronger viscosity-temperature dependence, convection experiments show that the cold upper thermal boundary layer may form a stagnant, rigid lid over a convecting interior, as is believed occurs in the planet Mars.

Convection theory therefore goes some way towards explaining the occurrences of divergent and convergent boundaries in the lithosphere together with the long aspect ratio of plates required. Convection theory also predicts that there should be topographic variations at the surface due to upwellings (high topography) and downwellings (low topography). This topographic signal needs to be separated from the topographic effects of density and thickness variations in the lithosphere. The topography remaining after the removal of

isostatic effects originating within the lithosphere from the observed topography is commonly referred to as *dynamic topography* and is discussed in further detail in §5.2.

5.1.4 Seismic tomography

Very detailed velocity models of the mantle can be constructed using seismic tomography. Seismic tomography is a technique using many measurements of seismic wave arrivals at a network of recording stations to construct a best-fitting three-dimensional model of the **S**-wave velocity structure of the upper mantle or the **P**-wave velocity structure of the lower mantle (Dziewonski & Woodhouse 1987; Su *et al*. 1994; Kárason & van der Hilst 2000; Nolet 2008). By computing slices at different depths, it is possible to see how the velocity structure varies as a function of depth within the mantle. The velocity structure most likely reflects density differences, which in turn reflect temperature differences, but may also reflect compositional heterogeneity. Near the surface ($y = 50$ km), the velocity structure is dominated by the presence of the continental and oceanic plates, the continental shields being fast and the mid-ocean ridges being slow. The effects of the overlying plates are lost beneath a certain depth in the mantle, but this depth is surprisingly large. A distinctive 'slow' seismic structure can be related to overlying oceanic ridge systems down to at least 1000 km (Su *et al*. 1994; Cadek *et al*. 1995). The remnants of old lithospheric slabs have also been detected from their effect on seismic velocities down to more than 1000 km (Wen & Anderson 1995). The correlation with plate tectonics is lost at 1500–1700 km, but at about 2000 km, the surface tectonic pattern can once again be weakly recognised from seismic tomography. In this region of the lower mantle, major mantle plumes and remnants of old lithosphere can be detected from seismic heterogeneities. This suggests that plumes originate close to the core–mantle boundary. It also suggests that this region is a graveyard for deeply subducted lithospheric remnants. Two 'megaplume' structures can be detected in the lower mantle below 2000 km. These major upwellings in the lower mantle are correlated with an abundance of hotspots on the Earth's surface, and are thought to be long-lived, stable flow structures. The presence of lower-mantle megaplumes, hotspots, mid-ocean ridges, subduction zones and remnant lithospheric slabs have been explained as the dynamic consequences of a mantle with a strong viscosity stratification (Fig. 5.5a, b).

5.1.5 Plate mode versus plume mode

Davies (1999) distinguished between a type of convection driven by the upper cooled thermal boundary layer ('plate mode') and a type driven by processes at the hot lower thermal boundary layer ('plume mode'). The recognition of different modes of convection helps to solve the puzzle of the relationship between the movement and boundaries of plates and the circulation in the convecting mantle.

The 'plate mode' is the mode of convection driven by the negative buoyancy of subducting oceanic plates. Plates are part of the underlying convection system, and their negative buoyancy drives convection, so they are active rather than passive components in an integrated plate-mantle system. Plates are sufficiently strong, owing to the temperature-dependence of rheology (§2.3), that they normally resist 'dripping' downwards by their negative buoyancy. Since we know that subduction is commonplace, there must be a factor causing downward flow of plates, such as the existence of zones of weakness (for instance, major faults). The position of plate boundaries therefore controls the locations of passive upwellings at spreading centres and downwellings at subduction zones. In this sense, surface plate motion 'organises' deeper mantle flow, a phrase coined by Brad Hager.

The life cycle of an oceanic plate begins at a spreading ridge, where mantle cools by conduction and thickens as it moves away horizontally (§2.2.7). The plate returns to the mantle, where it subducts and heats up by absorbing heat from its surroundings, thereby cooling the Earth's interior. The mantle loses most of its internal heat by this plate cycle, the remainder (about 10%) being lost by conduction through the continental lithosphere. The dominance of mantle flow organised by plate movement is seen in the topography associated with this plate-scale flow – the mid-ocean ridges elevated at kilometres above the adjacent ocean floor.

The 'plume mode', in contrast, is driven by the upwelling of positively buoyant material from the lower thermal boundary layer of the mantle. Many mantle plumes appear to be fixed in position relative to each other and are unrelated to the motion of the plates and to present-day plate boundaries. Although there are between 40 and over 100 volcanic hotspots (Burke & Wilson 1976; Crough & Jurdy 1980; Morgan 1981) (Table 5.1), not all of these are associated with plumes originating from the core–mantle boundary. Topographic swells in the ocean, however, such as the 2000 km-wide Hawaiian swell, can only be satisfactorily explained by the presence of a column of buoyant material beneath the lithosphere, and the association with volcanic activity supports the idea that this buoyant material is hot. Many postulated plumes have a present-day distribution correlated with the two major geoid highs (§5.1.6) in the Pacific and under Africa (Burke & Torsvik 2004; Burke *et al*. 2008) (Fig. 5.6). Other hotspots are within 1000 km of the edge of continents and may be related to a smaller scale of convective circulation driven by the step in the base of the lithosphere (King 2007) (Figs 5.6, 5.7) (§5.2.4).

Plumes transport heat from the interior of the Earth to the lithosphere. If the plume is envisaged as a vertical cylinder with radius r, with material flowing at velocity u, then the buoyancy flux B is

$$B = g\Delta\rho\pi r^2 u \qquad [5.8]$$

where $\Delta\rho$ is the density deficit between the plume material and the ambient mantle. Buoyancy flux therefore scales on the discharge of plume material and its density deficit. The buoyancy fluxes of the world's major volcanic hotspots are shown in Table 5.1. The buoyancy flux is closely related to the topographic expression of the swell – the largest swells are supported by the largest buoyancy fluxes, Hawaii being the largest. Estimates of the total heat transport by all known plumes (Davies 1988; Sleep 1990) suggest that plumes account for about 6% of global heat flow, which is similar to estimates of the heat transport out of the core (Stacey 1992). This supports the notion that plumes originate from the thermal boundary layer at the base of the mantle. Hotspots confidently related to mantle plumes have on average twice the buoyancy flux of hotspots that are candidates for edge-driven convection.

A physical manifestation of the plume mode is the flood basalt provinces, from which volcanic hotspot tracks emerge, such as the Chagos–Laccadive Ridge extending southwards from the Deccan Traps of western India to the present-day volcanic centre of Réunion Island in the Indian Ocean (Fig. 5.8). Flood basalts (§5.3.2, §5.3.3), or Large Igneous Provinces (LIPs), may extend up to 2000 km across, and may be several kilometres thick, so total volumes of extrusive eruptions range up to 10 million km^3. The LIPs and tracks are

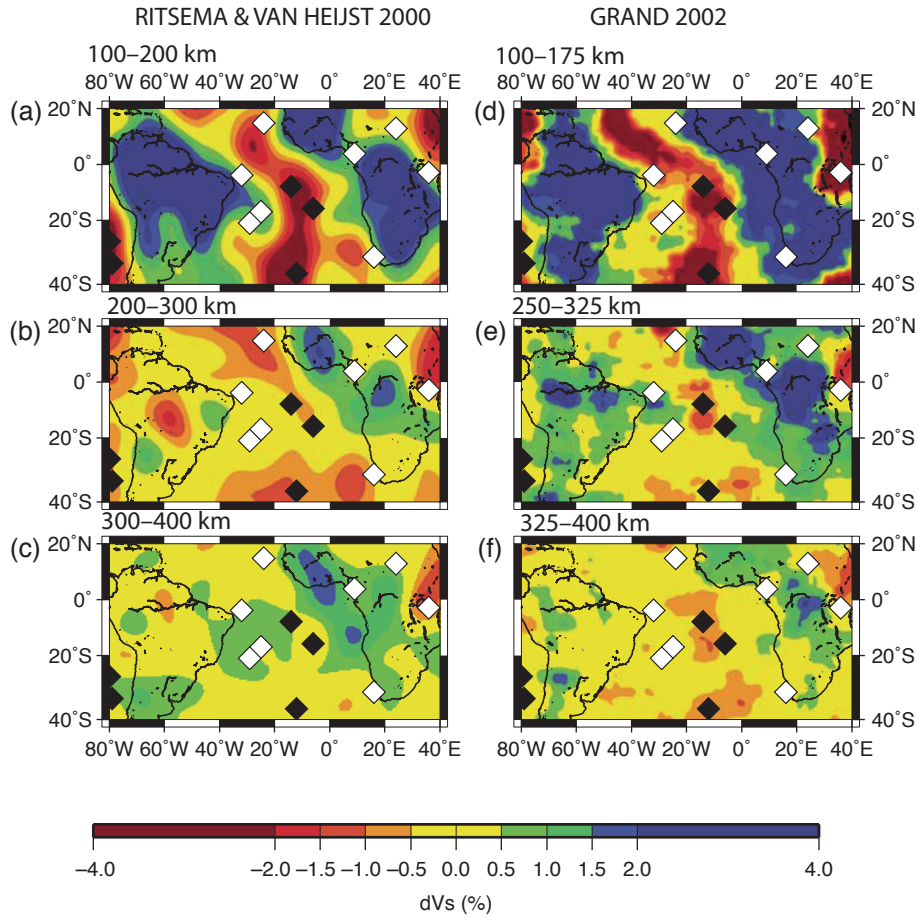

Fig. 5.6 S-wave tomography of the South America-Atlantic-Africa region from Ritsema & van Heijst (2000) (left) and Grand (2002) (right) for three depth slices, with hotspots shown as black and white diamonds from Sleep (1990), from King (2007). White diamonds are located where edge-driven convection is favourable geometrically, whereas black diamonds are in unfavourable positions geometrically. Colour scheme is based on the percentage departure from a mean velocity dVs.

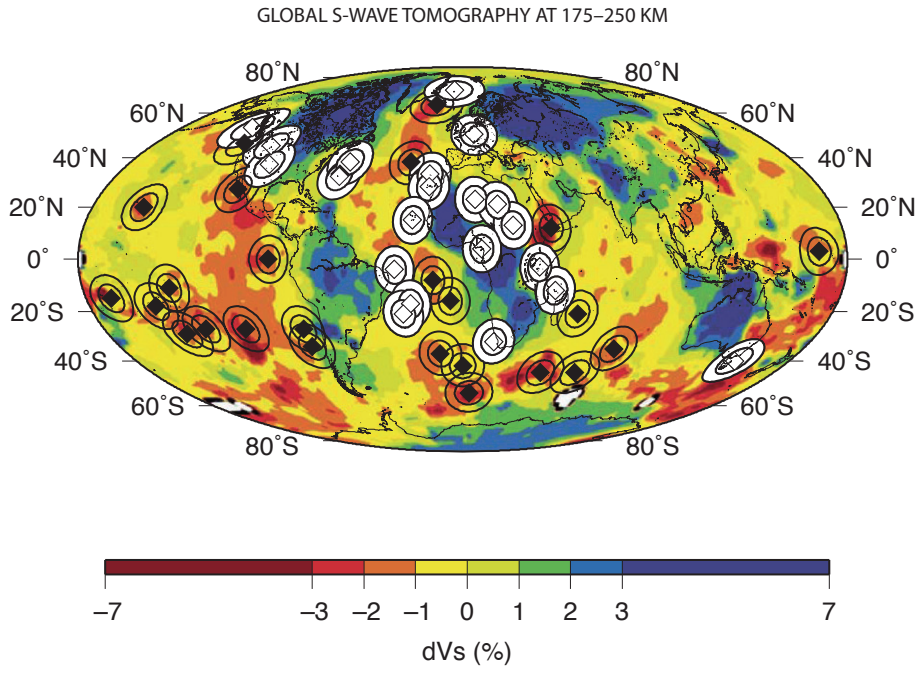

Fig. 5.7 Global S-wave tomography from Grand (2002) for the 175–250 km depth slice, showing hotspots from Sleep (1990), with circles of radius 660 km and 1000 km drawn around the centre of the hotspot. Candidates for edge-driven convection (EDC) are those where the circle intersects a blue (fast) anomaly, shown in white. After King (2007).

Table 5.1 World's major hotspots, with buoyancy flux, after Sleep (1990), Turcotte and Schubert (2002), and Davies (1988), classified according to whether the upwelling is related to edge-driven convection or deeper plumes, based on: (i) Courtillot *et al*. (2003); (ii) Montelli *et al*. (2003); and (iii) King (2007). Those marked (4) are tentatively assigned to EDC based on their spatial proximity to a continental edge, but some of this category may be plume-related. Based on this classification, the average buoyancy flux for plume-generated hotspots is 1.7 $Mg s^{-1}$ and for EDC is 0.86 $Mg s^{-1}$

Hotspot	Flux ($Mg s^{-1}$) Sleep 1990/Turcotte & Schubert 2002 p. 261/Davies 1988	Location-type 1 – Courtillot *et al*. 2003; 2 – Montelli *et al*. 2003; 3 – King 2007
Afar, African plate	1.2/1.2/-	Plume-generated[1,2,3]
Ascension, South American plate	-/0.9/-	Plume-generated[2,3]
Australia, East, Indo-Australian plate	0.9/0.9/-	Edge-driven[4]
Azores, Eurasian plate	1.1/1.1/-	Plume-generated[2,3]
Balleny, Antarctic plate		Edge-driven[4]
Baja, eastern Pacific	0.3/0.3/-	Edge-driven[4]
Bermuda, North American plate	1.1/1.3/-	Edge-driven[3]
Bouvet, African plate	0.4/0.4/-	Plume-generated[1]
Bowie seamount, Pacific plate	0.3/0.6/-	Edge-driven[3]
Canary, African plate	1.0/1.0/-	Edge-driven?[3] Plume-generated[2]?
Cape Verde, African plate	1.6/1.0/-	Edge-driven[3]
Caroline Islands, Pacific plate	1.6/1.6/-	Plume-generated[1]
Comoros, African plate		Edge-driven[4]
Crozet, Antarctic plate	0.5/0.5/-	Plume-generated[2,3]
Darfur, African plate	-/0.4/-	Plume-generated[1]
Discovery, African plate	0.5/0.6/-	Plume-generated[1]
East African, African plate	-/0.6/-	?Edge-driven[4]
Ethiopian, African plate	-/1.0/-	?Edge-driven[4]
Easter, Nazca plate	3.3/3.3/-	Plume-generated[1,2,3]
Eifel, Eurasian plate		Plume-generated[2]
Fernando, South American plate	0.5/0.7/0.9	Edge-driven[3]
Galapagos, Nazca plate	1.0/1.0/-	Plume-generated[1]
Great Meteor seamount (New England), African plate	0.5/0.4/0.4	Plume-generated[1]
Hawaii, Pacific plate	8.7/7.4/6.2	Plume-generated[1,2,3]
Hoggar, African plate	0.9/0.6/0.4	Edge-driven[3]
Iceland, Eurasian plate	1.4/1.4/-	Plume-generated[1,2,3]
Jan Mayen, Eurasian plate		Edge-driven[3]
Juan de Fuca/Cobb seamount, Pacific plate	0.3/0.3/-	Edge-driven[4]
Juan Fernandez, Nazca plate	1.6/1.6/1.7	?Edge-driven[4]
Kerguelen, Antarctic plate	0.5/0.4/0.2	Plume-generated[1,2,3]
Lord Howe, Indo-Australian plate		Edge-driven?[4]
Louisville, Pacific plate	0.9/2.0/3.0	Plume-generated[1,2,3]
Macdonald seamount, Pacific plate	3.3/3.6/3.9	Plume-generated[1]
Madeira, African plate		Edge-driven[3]
Marquesas Islands, Pacific plate	3.3/4.0/4.6	Plume-generated[1]
Marion, Antarctic plate		Plume-generated[1]
Martin	0.5/0.6/0.8	
Meteor, African plate	0.5/0.4/0.4	Plume-generated[1]
Mount Cameroon, African plate		Edge-driven[3]
Pitcairn, Pacific plate	3.3/2.5/1.7	Plume-generated[1]
Raton, North American plate		Edge-driven[3]
Réunion, African plate	1.9/1.4/0.9	Plume-generated[1,2,3]
St Helena, African plate	0.5/0.4/0.3	Edge-driven[3]
Samoa, Pacific plate	1.6/1.6/-	Plume-generated[1,2,3]
San Felix, Nazca plate	1.6/2.0/2.3	Edge-driven[4]
Socorro, Pacific plate		Edge-driven[3]
Tahiti, Pacific plate	3.3/4.6/5.8	Plume-generated[2,3]
Tasman, Central, Indo-Australian plate	0.9/0.9/-	Edge-driven[3]
Tasman, East, Indo-Australian plate	0.9/0.9/-	Edge-driven[3]
Tibesti, African plate	-/0.3/-	Edge-driven[3]
Trindade, South American plate		Edge-driven[3]
Tristan, African plate	1.7/1.1/0.5	Plume-generated[1,2,3]
Vema seamount, African plate	-/0.4/-	Edge-driven[3]
Yellowstone, North American plate	1.5/1.5/-	Edge-driven[3]

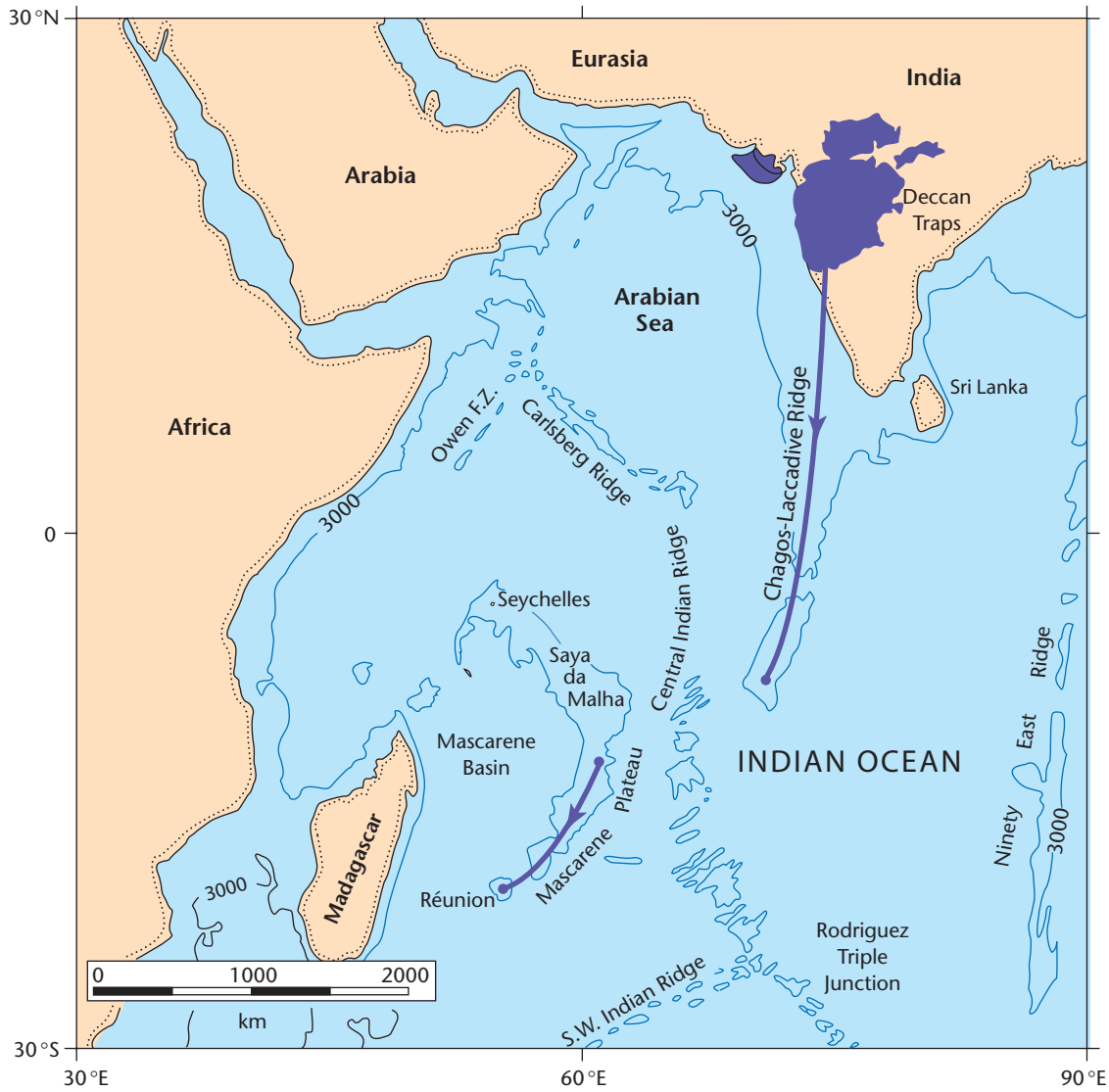

Fig. 5.8 The path of the Réunion hotspot track in the Indian Ocean and the Deccan flood basalt province. After White & McKenzie (1989), reproduced with permission of the American Geophysical Union.

explained (Morgan 1981; Richards *et al.* 1989; Griffiths & Campbell 1990) as due to the arrival of a plume head, followed by a plume tail as the overlying plate moves away from the conduit. The track shows the path of the overlying plate over the plume tail, ending at the present-day volcanic centre (Fig. 5.9).

It is unlikely that material of normal mantle composition can generate >1 million km^3 of extrusive basalts from melting of a plume head. An additional important factor may be the presence of a higher basaltic composition in the plume head, perhaps due to entrainment of previously subducted oceanic crust (Hoffman & White 1982), which would lower the solidus temperature. Other possibilities are higher plume temperatures, or lithospheric thinning (Chapter 3) caused by the impingement of the plume on the base of the plate.

In summary, the presence of topographic swells, and LIPs connected to active volcanic centres by hotspot tracks, can best be explained by the rise of long-lived columns of buoyant mantle material 200–300 °C hotter than the surrounding mantle. The rise of these mantle plumes most likely takes place from the lower hot boundary layer of the mantle and contributes to the 'plume mode' of mantle convection. Since the distribution of hotspots shows no relation to present-day plate boundaries, the plate mode and the plume mode of convection do not appear to be strongly coupled (Stefanik & Jurdy 1994).

5.1.6 The geoid

Measurements of the Earth's gravity field also provide much information about the dynamics of the mantle. Numerical simulations of convection in the upper mantle (McKenzie *et al.* 1980) show that upwellings and downwellings should be accompanied by variations in the sea surface (amplitude of up to 10 m) and in the gravity anomaly (amplitude of up to 20 mgal) (Fig. 5.10). The geoid is the

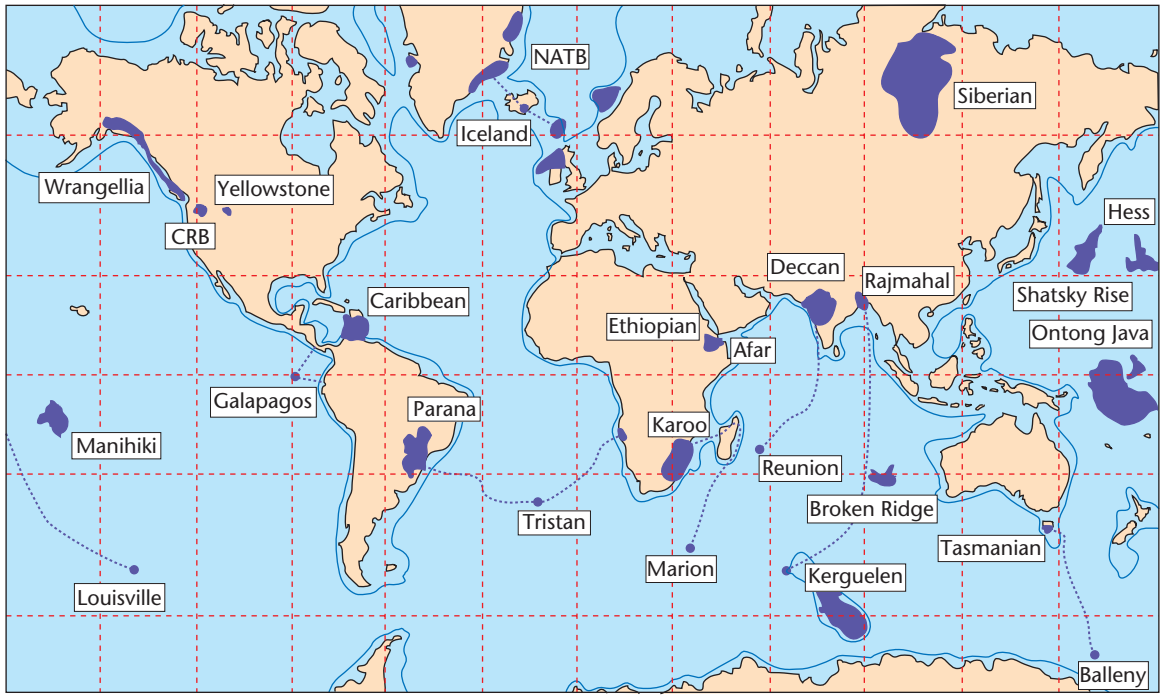

Fig. 5.9 Map of oceanic and continental flood basalt provinces and hotspot locations. Dashed lines connect flood basalt provinces with present-day volcanic centres (volcanic hotspots), representing hotspot tracks. The Chagos–Laccadive Ridge joining the Deccan with Réunion is discussed in the text. Hotspots are concentrated on and around geoid highs (Fig. 5.7). CRB, Columbia River Basalt province; NATB, North Atlantic Tertiary Basalt province. From Duncan & Richards (1991) (fig. 11.12 of Davies 1999), reproduced with permission of John Wiley & Sons, Inc.

gravitational equipotential surface around the Earth and has the form of an oblate spheroid (§1.4.2). Departures from the reference geoid due to the non-uniform distribution of mass within the Earth are called geoid height anomalies. Upwellings have positive gravity anomalies and an elevated sea surface (positive geoid height anomaly), whereas the reverse is true of the downwellings. This is at first contradictory. We should expect a density excess at depth to cause a geoid high and a positive free-air anomaly, and a density deficit should produce a geoid low and a negative free-air anomaly. However, the free surface is deflected upwards over the rising limbs of the convection cells, and downwards over the descending limbs. This outweighs the effects of the density differences. The net result is that rising limbs are associated with geoid highs and positive free-air anomalies.

A global map of the geoid anomaly (Lemoine *et al.* 1998) (Fig. 1.12) shows maximum geoid anomalies of approximately 100 m, with highs in the southwestern Pacific (+80 m) and northern Atlantic (+60 m), and lows in the Indian Ocean (−100 m), Antarctica and Southern Ocean (−60 m) and the western Atlantic Ocean and adjoining American continent (−40 m). Although some of the geoid pattern is related to plate tectonic processes such as subduction (see §5.2.2), many of the geoid height anomaly features cannot be explained in this way and reflect deeper processes in the mantle.

It was recognised at an early stage (e.g. Runcorn 1967) that zones of plate convergence are generally associated with highs in the observed long-wavelength geoid. For example, the major subduction zones of the Earth all have geoid highs (Chase 1979). The long-wavelength (degree <10[1]) geoid anomalies are broadly comparable to those expected from the excess density of seismically active, cold subducted slabs. However, the geoid anomaly depends not only on the 'driving' density contrasts at depth, but also on the viscosity structure of the mantle. This is because the density contrasts, such as due to chemical layering, set up flows causing a deformation of the boundaries of any density contrast, the amplitude of which depends on the viscosity structure. Incorporating dynamic effects, the presence of high-density material in the upper mantle (such as due to subducted lithosphere) should lead to long-wavelength geoid highs. But the presence of dense material in the lowermost mantle should lead to long-wavelength geoid lows. Consequently, long-wavelength geoid highs can be associated with high-density material (old slabs) in the upper mantle and low-density material (megaplumes) in the lower mantle. Hager (1984) found that the geoid anomalies (at degree <10) associated with subduction could best be explained by a dynamic model in which the density effects of subducting slabs penetrated deep into the lower mantle (through the 670 km discontinuity) and in which the viscosity contrast between upper and lower mantle was of the order of 50 to 100.

Subtracting the estimated effects of subduction (the so-called 'slab geoid') from the observed geoid reveals the *residual geoid* (Crough

[1]Wavelength is normally expressed in terms of spherical harmonic degree l. For degree l, there are l wavelengths in the circumference of the Earth. At degree 2, there are just two hemispherical highs and lows.

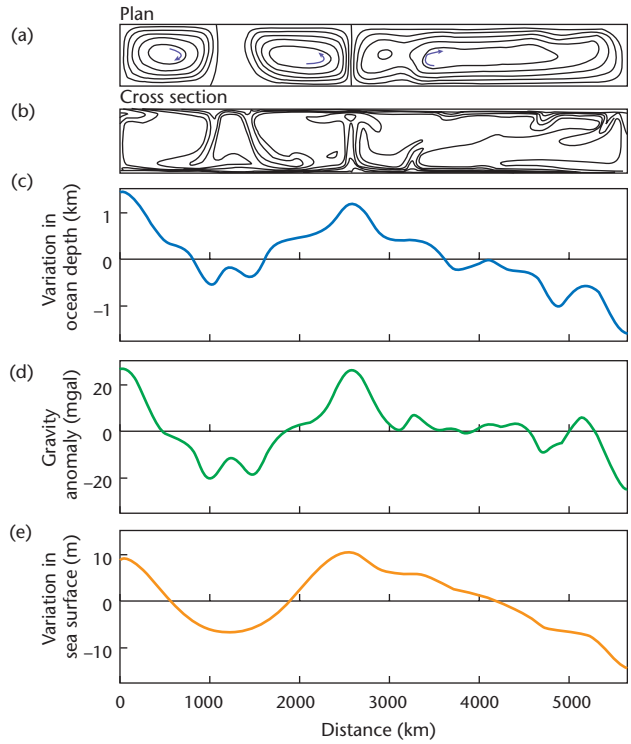

Fig. 5.10 Computer modelling of convection in an upper mantle with constant viscosity heated from below. (a) and (b) Temperature field contoured at 100 °C intervals, showing three upwellings and two downwellings in plan and cross-section; (c) variation in depth of the ocean floor; (d) variation in the gravity anomaly; and (e) variation in height of the sea surface (geoid height anomaly) resulting from the convection pattern in (a) and (b). Reproduced from McKenzie *et al*. (1980) by permission from Macmillan Publishers Ltd.

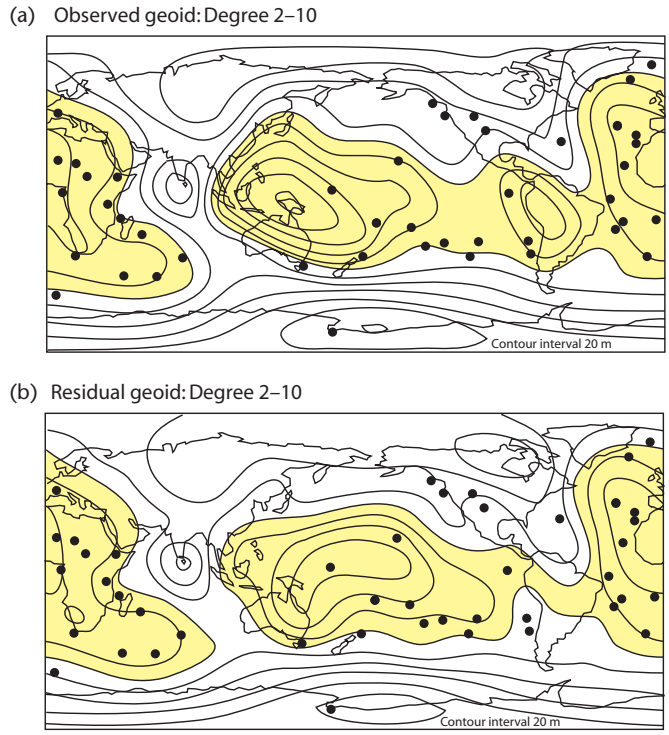

Fig. 5.11 Observed (a) and residual (b) long-wavelength geoid at degree 2–10 (Lerch *et al*. 1983; Hager 1984), contoured at a 20 m interval. Geoid highs are shaded. The residual geoid is obtained by subtracting a dynamically consistent slab geoid from the observed geoid. The distribution of surface hotspots, sites of intraplate volcanism, and anomalous plate volcanism (black dots) shows a correlation with geoid highs.

& Jurdy 1980; Hager 1984) (Fig. 5.11). It is noticeable that there is a residual geoid high along a nearly continuous E–W band, with a maximum in the Pacific Ocean and a secondary peak over Africa. This pattern may reflect megaplume activity in the lower mantle. The correlation of residual geoid highs with the location of hotspots supports this view.

In summary, the pattern of geoid anomalies is highly diagnostic of the processes of slab subduction and mantle convection. The challenge for us is how to make the connection between deep sublithospheric processes and basin development on the continents.

5.2 Surface topography and bathymetry produced by mantle flow

5.2.1 Introduction: dynamic topography and buoyancy

The term '*dynamic topography*' is defined as 'the vertical displacement of the Earth's surface generated in response to flow within the mantle' (Richards & Hager 1984). It is therefore distinct from isostatic topography generated by near-surface density contrasts such as due to crustal thickness changes.

Nevertheless, as pointed out by Davies (1999), there is some confusion over what dynamic topography really is and how it differs from the topography resulting from a simple isostatic balance. If we accept that the oceanic tectonic plates constitute an upper, cooled, thermal boundary layer, then because these plates are actively participating in a global convection system, the surface elevation of the oceanic plates represents dynamic topography. That is, the increasing bathymetry of the ocean floor from the spreading centre to the abyssal plain (§2.2.7) is dynamic topography dominated by the effect of cooling of the upper thermal boundary layer. The bathymetry of the ocean floor is, however, calculated using an isostatic balance, neglecting the viscous stresses set up by three-dimensional variations in buoyancy. Ambiguously, therefore, dynamic topography results from a purely static balance.

The broad oceanic swells and their continental counterparts are thought to be associated with underlying upwellings of mantle flow structures and clearly constitute 'dynamic topography'. The less easily demonstrable topographic changes associated with smaller scales of convection are also clearly 'dynamic'.

Other situations exist where cooling takes place, but where it is not related to the Earth's convection system, such as following mechanical stretching of the lithosphere, or surrounding a large intrusion in the crust. The topographic effects of these processes can also be calculated by an isostatic balance, but such topography is not 'dynamic'.

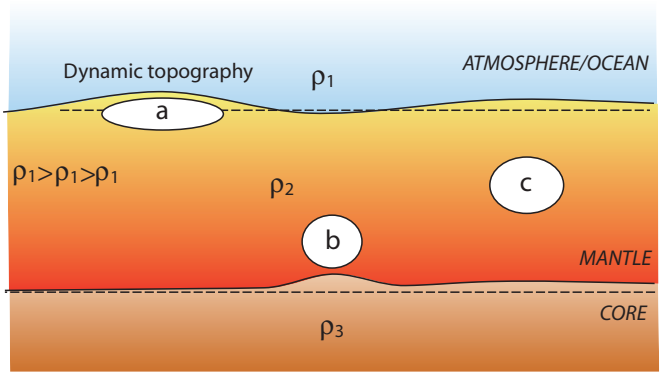

Fig. 5.12 Schematic diagram showing effect of buoyant blobs on the upper and lower surfaces of a fluid layer, which are assumed to be free to deflect vertically. A less dense fluid (such as the atmosphere or oceans) overlies the upper surface, and a denser fluid (core) underlies the lower surface. Adapted from Davies (1999, p. 234, fig. 8.5), © Cambridge University Press, 1999.

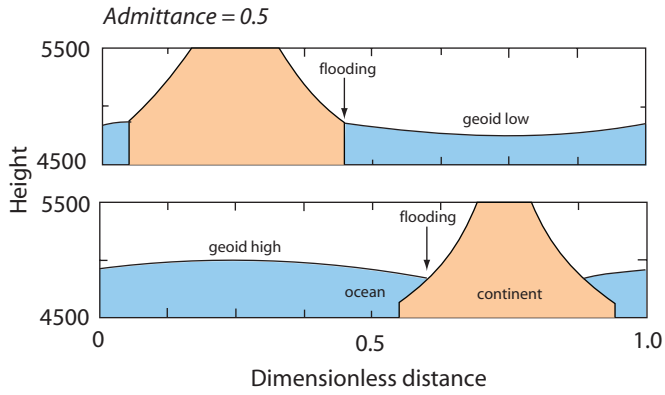

Fig. 5.13 Topography of continents and elevation of sea surface, showing degree of continental flooding when the continent is positioned over a geoid high (top), and geoid low (bottom). Admittance is 0.5, maximum geoid is 100 m. The topography of the continent is the result of isostasy, dynamic topography and seawater loading. The continent experiences a greater amount of flooding when it is positioned over a geoid low. After Gurnis (1990a), reproduced with permission of American Association for the Advancement of Science.

Turning to other mechanisms, topography may result from the subduction of cold oceanic slabs into the hot mantle, setting up a large-scale flow, in which case the topography is 'dynamic'. But the regional bending of the oceanic plate beneath the ocean trench, and the regional bending of the retro-arc region of the continental plate in an ocean–continent convergence zone, are due to flexure of the elastic lithosphere (Chapter 4), are not linked to the underlying convection system, and are not 'dynamic'.

The fact that the bathymetry of oceanic plates can be explained by a cooling plate model (§2.2.7) shows that there is no recognisable influence of deeper mantle convection in the elevation of the ocean floor. The submarine topography is explainable using the plate mode of convection (§5.1.5). Numerical convection models can produce topography that matches observed seafloor bathymetry well; this topography is due to cooling in the upper thermal boundary layer of the convection system. The dynamic topography associated with subduction, however, is much more difficult to model, since numerical models include an artificial, local weakening of the viscosity structure to simulate a subduction zone fault, and the predicted topography is highly sensitive to details of the deeper viscosity structure and of the plate thickness approaching the subduction zone, both of which are poorly constrained.

The underpinning concept for the role of mantle dynamics in forming surface topography is that buoyancy drives convective flow and causes a deflection of the surfaces of the fluid layer undergoing motion. The distribution within the fluid layer of the sources of buoyancy, which we can call 'blobs', is critical to the topographic deflection (Fig. 5.12) (Davies 1999). For example, if the blob is close to the upper surface, its buoyancy must be opposed by a gravitational force acting on the upward deflected surface. The downward-acting weight of the upward deflected surface counterbalances the upward-acting buoyant force of the blob. This is a static force balance with no momentum. If the blob is located close to the lower boundary, the lower boundary is deflected upwards but the upper surface is barely deflected since it is too far away to be affected by the viscous stresses transmitted by the blob. If the blob is situated in the centre of the fluid layer, it may deflect both the upper and lower layers. The dynamic topography of the Earth's surface therefore carries important information about the distribution of buoyancy and therefore about convection in the interior of the Earth.

As introduced above, when a viscous fluid is disturbed by the presence of a parcel of material with positive buoyancy, viscous stresses are set up that cause the free surface to move upward (Fig. 5.12). The response time of the mantle to a disturbance is dependent on its viscosity (estimated from glacial rebound studies, see §2.2.8, §4.1.1) and the wavelength of the parcel of positive buoyancy (Zhong *et al.* 1996). For mantle flow related to subduction, with a wavelength of $1–3 \times 10^3$ km (Gurnis 1992, 1993; Burgess & Gurnis 1995) the time scale is 10^4 yr, and for larger wavelengths of anomaly ($>5 \times 10^3$ km), such as expected under insulating supercontinental assemblies (Anderson 1982; Gurnis 1988), the response time is up to 10^5 yr (Gurnis *et al.* 1996). The mantle can therefore be considered as responding effectively instantaneously to the disturbance by a positive buoyancy parcel.

The dynamic topography associated with the long-wavelength heterogeneities identified by seismic tomography should theoretically be large (>1000 m, Hager & Clayton 1989) in order to explain the undulations in the geoid. However, dynamic topography of this scale has not been detected (Le Stunff & Ricard 1995). A number of studies suggest that the global scale variations in dynamic topography, corrected for effects within the lithosphere, are in the range 300–500 m (e.g. Cazenave *et al.* 1989; Nyblade & Robinson 1994). However, variation in the degree-2 geoid is about 50 m (Hager *et al.* 1985).

The ratio of geoid to dynamic topography is termed *admittance*. Although a continent may be located over a geoid high, which therefore has elevated water levels in the ocean, the greater dynamic topography in this region may cause subaerial emergence rather than flooding (Fig. 5.13). The admittance is therefore important in studying continental flooding histories (Gurnis 1990a). For low admittance, flooding takes place preferentially over geoid lows. At high

values of admittance, the continent may be flooded preferentially over geoid highs. The flooding history of the North American continent during the Phanerozoic (maximum of 30% of the continental surface) (Bond 1979) indicates that since the geoid should lie within the range 0–100 m, the amplitude of dynamic topography must be up to 150 ± 50 m.

The recognition of the amplitude and wavelength of dynamic topography at the Earth's surface at the present day is made difficult by the isostatic compensation of strong crustal and lithospheric thickness and density variations. If these isostatic effects could be removed from the Earth's topographic field, we should obtain the dynamic component attributable to mantle flow. When this 'residual' topography is mapped globally, it shows a pattern of long wavelengths of up to several thousand kilometres and heights of up to 1 km (Fig. 5.14) (Steinberger 2007). Secondly, we could estimate dynamic topography using a density model of the mantle derived from tomographic studies (§5.1.4) (Moucha *et al.* 2008). Such estimates are broadly in line with the estimates derived from 'residual' topography.

In the following paragraphs, we examine the dynamic topography associated with different geodynamic situations. First, we consider the subduction of cold oceanic slabs, particularly those that subduct at shallow angles (Mitrovica *et al.* 1989; Gurnis 1993; Spasojevic *et al.* 2008). Second, we look at the very large-scale dynamic topography associated with supercontinental assemblies (Anderson 1982). Third, we reduce scale and speculatively consider small-scale convection associated with edges and steps beneath the continental lithosphere (King & Anderson 1998). Fourth, we evaluate the dynamic topography associated with mantle plumes and superplumes (Lithgow-Bertelloni & Silver 1998).

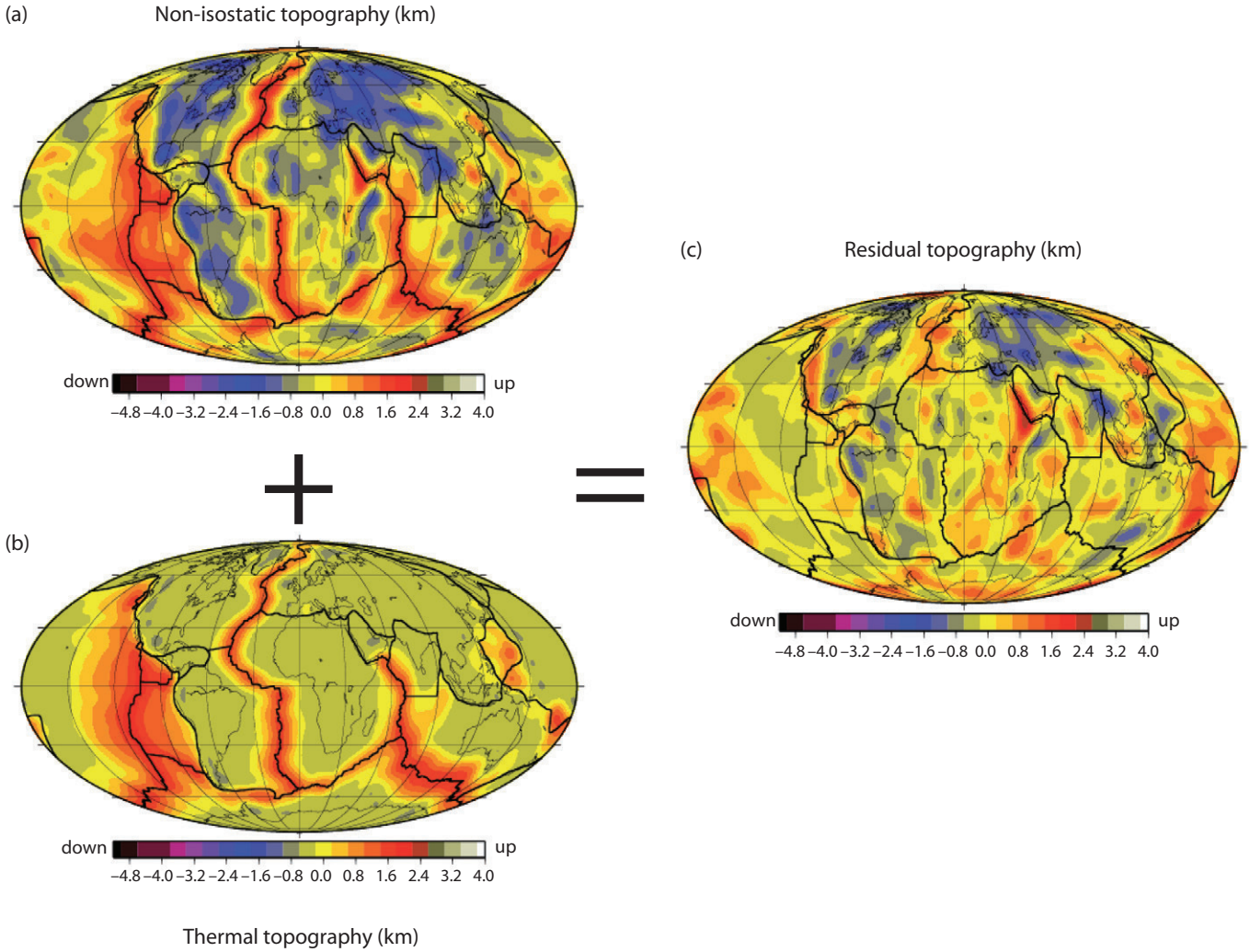

Fig. 5.14 Global dynamic topography based on residual topography after removal of isostatic effects of crustal and lithospheric thickness changes and thermal topography due to the cooling of the ocean lithosphere (Steinberger *et al.* 2001). Part (a) is the non-isostatic topography after removing isostatic effects from the actual topography. Part (b) is the thermal topography calculated from the age_2.0 ocean floor age grid of Müller *et al.* (2008a) for ages less than 100 Ma. Part (c) is the residual topography calculated for an assumed global seawater cover, equivalent to dynamic topography thought to result from mantle circulation.

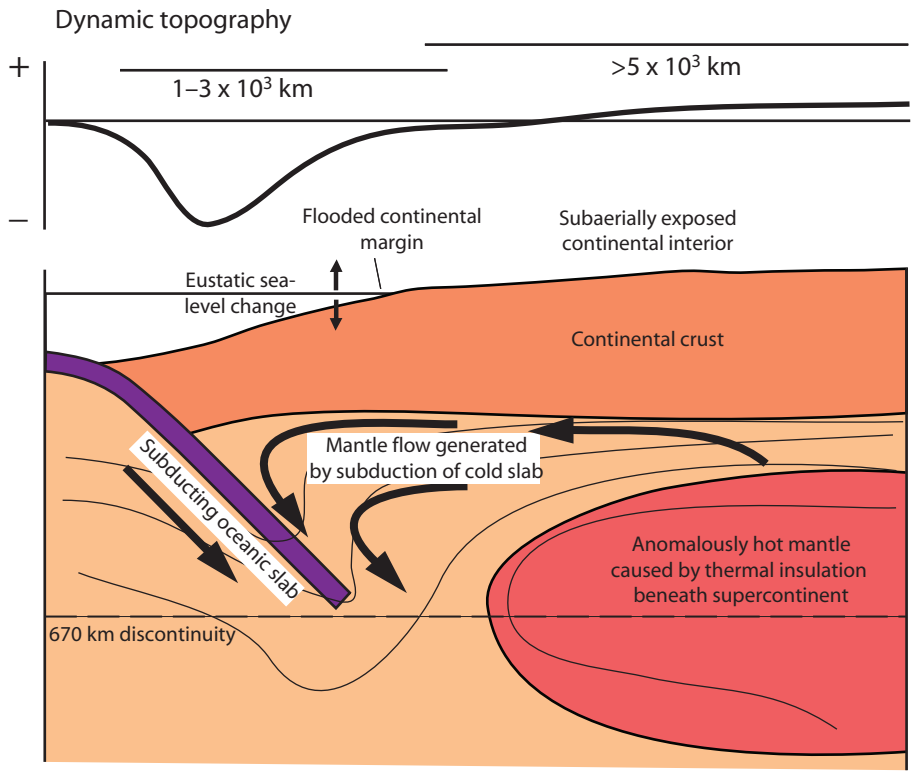

Fig. 5.15 Schematic diagram to show generation of dynamic topography from subduction of a cold oceanic slab (wavelength 1–3 × 10^3 km) and from mantle insulation beneath a supercontinent (wavelength >5 × 10^3 km) (after Burgess *et al*. 1997).

5.2.2 Dynamic topography associated with subducting slabs

If dynamic topography results from the thermal effects of flow in the mantle, we should be able to recognise dynamic topography behind ocean trenches where cold lithospheric slabs disturb the mantle temperature field (Parsons & Daly 1983; Mitrovica & Jarvis 1985; Gurnis 1992) (Fig. 5.15). The ramp-like tilting of the continents towards their oceanic active margins indicated by the preservation of extensive (>1000 km) wedge-shaped stratigraphic packages (see §5.4) has been taken to reflect dynamic topography above shallowly subducting ocean slabs on a number of continents, such as western North America (Mitrovica *et al*. 1989; Burgess *et al*. 1997), the Russian Platform (Mitrovica *et al*. 1996) and eastern Australia (DiCaprio *et al*. 2009).

Although the amplitude of dynamic topography behind subduction zones is controversial, the wavelength is thought to extend 1000–2000 km from the ocean trench into the continental plate. Consequently, dynamic topography may be recognised as a realm of subsidence extending far beyond the location of retro-arc foreland basins (Mitrovica *et al*. 1989; Catuneanu *et al*. 1997; Burgess & Moresi 1999).

Dynamic topography depressions of approximately 500 m are predicted by geoid models over subducting slabs (Hager & Clayton 1989). However, the measurement of dynamic topography behind trenches is problematic, since the dynamic topography must be separated from other forms of subsidence. One approach is to compare such regions with areas unaffected by slab-related dynamic topography. This can be done by a comparison of the distribution of topography (hypsometry) behind ocean trenches compared with a world average (Gurnis 1993). This suggests that regions within 1000 km of ocean trenches are depressed by 400–500 m in the western Pacific (Gurnis 1993). A second approach is to remove the isostatic effects of lithospheric thickness changes and thermal subsidence. A study of backarc regions of the southwestern Pacific (Wheeler & White 2000) indicated a maximum of 300 m of negative long-wavelength (c.10^3 km) dynamic topography (Fig. 5.16).

Since there must be major uncertainties in the estimation of dynamic topography behind ancient subduction zones, a first approach to the modelling of dynamic topography in basin analysis is to use an expression for the geometric form of the dynamic topography by assuming that it is made of two components (Gurnis 1992; Coakley & Gurnis 1995; Burgess & Gurnis 1995): (i) an exponential component with an exponent λ and maximum deflection f_m; and (ii) a linear tilt with a maximum gradient α in m km^{-1} and a maximum distance from the trench at which tilting occurs η. Combining these components gives

$$f(x) = f_m\left(e^{-x/\lambda}\right) + \alpha(\eta - x) \qquad [5.9]$$

where x is the horizontal orthogonal distance from the trench.

With eqn. [5.9] we are able to approximate the dynamic topography as a function of distance from the trench axis and to consider its impact on the surface elevation of the retro-arc region of a continent as a thought experiment. We initially take the following parameter values: $\lambda = 200$ km, $f_m = 2000$ m, $\alpha = 0.5$ m km^{-1}, and $\eta = 2000$ km. If we superimpose on this distribution of dynamic topography $f(x)$ a realistic deflection due to flexure in the retro-arc

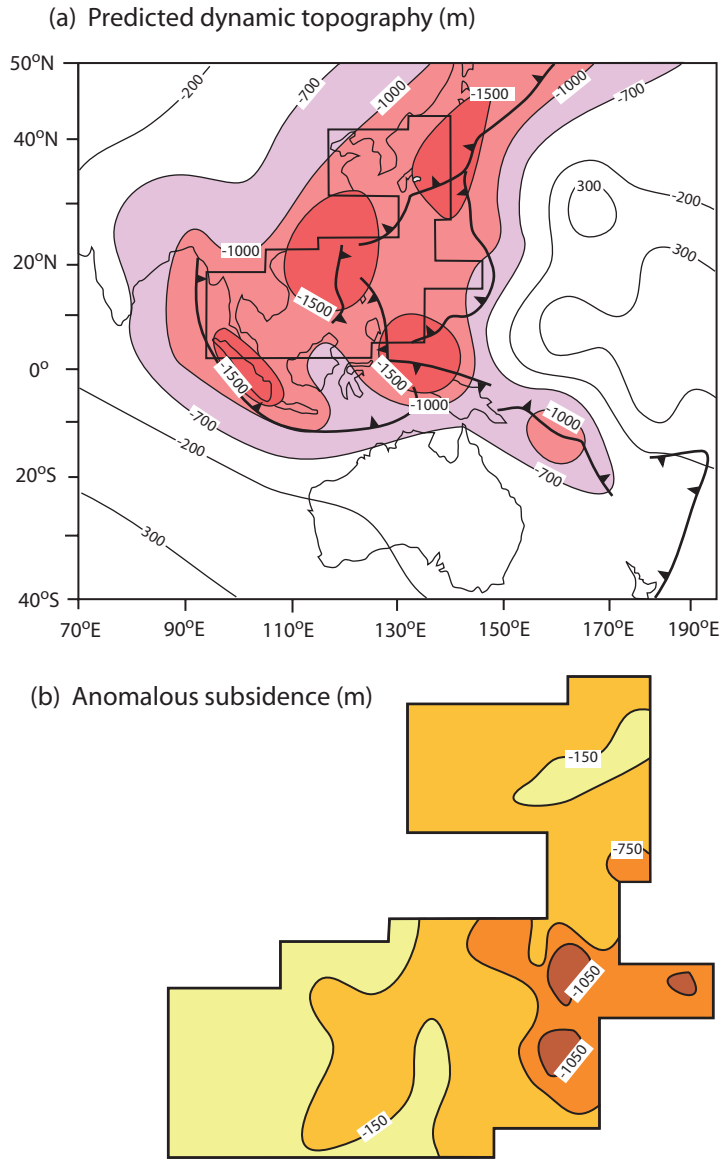

Fig. 5.16 (a) Predicted dynamic topography in SE Asia (Lithgow-Bertelloni & Gurnis 1997) using a history of subduction over the past 180 Myr. (b) The 'anomalous' subsidence after removal of isostatic effects related to basin formation by Wheeler & White (2000), showing that the observed dynamic topography is significantly less than predicted by slab models.

region $w(x)$, it is apparent that the dynamic topography is sufficient to exceed the effects of flexural forebulge uplift (Allen & Allen 2005, p. 179). Consequently, the back-bulge and flexural forebulge regions are zones of (transient) subsidence (Fig. 5.17a), as envisaged by DeCelles and Giles (1996). The parameter values used are similar to those used to model the Phanerozoic evolution of the North American craton (Burgess & Gurnis 1995). If, however, we take parameter values that more closely reflect recent estimates of the amplitude of dynamic topography behind trenches ($\lambda = 200$ km, $f_m = 500$ m, $\alpha = 0.2$ m km^{-1}, and $\eta = 2000$ km), the dynamic topography is insufficient to exceed the magnitude of forebulge uplift. Consequently, the flexural forebulge remains an erosional zone in the retro-arc region (Fig. 5.17b). If we reduce the maximum distance of tilt to 1000 km, which might result from a steepening of slab dip (see below), the dynamic topography reduces to such low values that the back-bulge region is most likely non-depositional while the forebulge is erosional (Fig. 5.17c). Clearly, the amplitude and wavelength of dynamic topography is extremely important to the preservation of forebulge and back-bulge stratigraphy (see also Burgess & Moresi 1999).

The horizontal distance into the upper plate affected by dynamic topography should be related to the dip of the subducting slab (Mitrovica *et al.* 1989). Shallow subduction angles of <45° are required to produce deflections of the continental plate >500 km from the ocean trench for a range of initial slab temperatures relative to the mantle of −200 K to −800 K. These initial temperature contrasts most likely reflect the age of the oceanic plate at the point of subduction. The vertical amount of dynamic topography, however, is determined by the temperature contrast between the

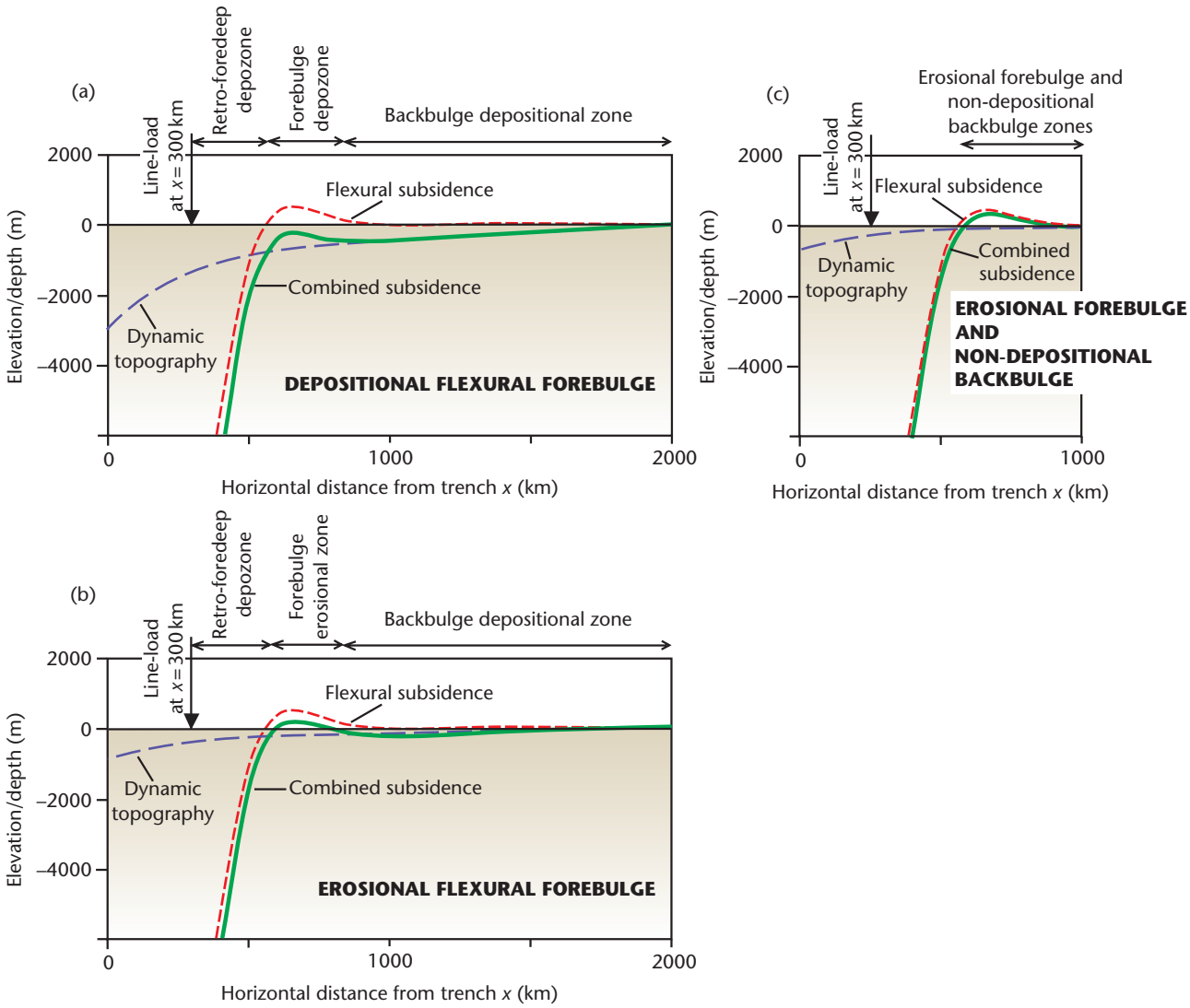

Fig. 5.17 Combination of flexural subsidence and dynamic topography behind subduction zones. In all cases, the flexural subsidence is that due to a line load at $x = 300$ km on a continuous plate with a flexural rigidity of 5×10^{23} Nm with a maximum deflection w_0 of 10 km. $\Delta\rho$ in the flexural parameter is 1300 kg m^{-3}. (a) Dynamic topography calculated using $f_m = 2000$ km, $\lambda = 200$ km, $\alpha = 0.5$, and $\eta = 2000$ km. The dynamic subsidence is large enough to overwhelm flexural uplift in the flexural forebulge region. (b) Dynamic topography calculated using $f_m = 500$ km, $\lambda = 200$ km, $\alpha = 0.2$, and $\eta = 2000$ km. Dynamic subsidence is sufficient to cause extensive backbulge deposition, but the flexural forebulge is erosional. (c) Dynamic topography calculated using $f_m = 500$ km, $\lambda = 200$ km, $\alpha = 0.2$, and $\eta = 1000$ km. Dynamic subsidence is insufficient to offset the effects of flexural forebulge uplift, and the backbulge region experiences such limited subsidence that it is likely to be non-depositional.

slab and the surrounding mantle, the flexural rigidity of the lithosphere, as well as the slab dip (Mitrovica *et al.* 1989). On cessation of subduction, any transient dynamic topography should be removed, the time scale of the uplift depending only on the initial temperature contrast between the slab and the mantle. 25 Myr is a typical recovery time for 95% of the uplift. There are therefore essentially two distinct modes of subduction, shallow and steep, that determine the dynamic subsidence of the continental interior behind ocean–continent boundaries, with secondary effects from plate age, rate of subduction, flexural rigidity, and viscosity structure of the upper mantle.

The evolution of dynamic topography through time may be complex. This is because the age of the oceanic slab, the velocity of plate subduction, and the angle of subduction change through time. The dips of slabs soon after the initiation of subsidence are believed to be close to vertical (Gurnis & Hager 1988). Over a period of perhaps 50 Myr, the slab shallows as a horizontal pressure gradient in the upper mantle develops (Stevenson & Turner 1977). The two most steeply dipping subduction zones in the Pacific, the Mariana and Kermadec, corresponding to young oceanic lithosphere, are both nearly vertical, whereas the oldest slab, Japan, has a dip of just 45°. Shallow slab dips may also be due to the attempted subduction

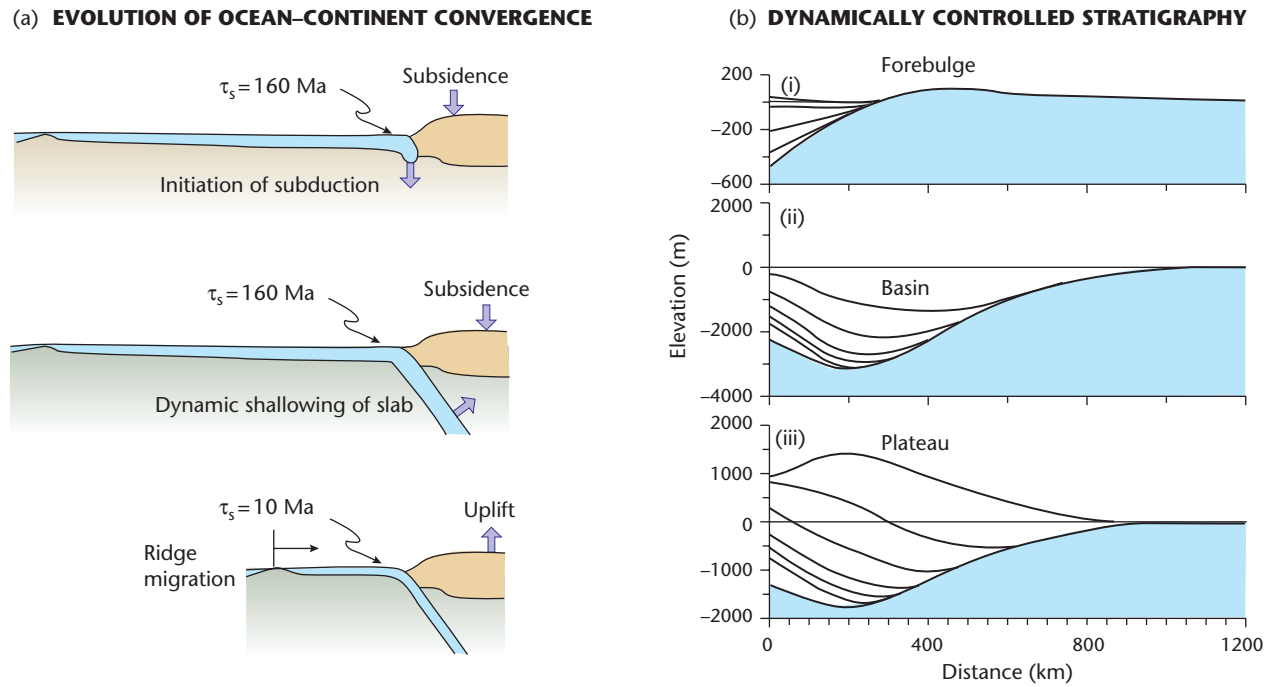

Fig. 5.18 Three stages in the evolution of dynamic topography over a subduction zone (a) and the associated chronostratigraphic surfaces in the region of the continental plate affected by dynamic topography (b). (i) An old (160 Ma) slab initially dips vertically, then penetrates the mantle by 100 km. The chronostratigraphic surfaces are separated by 2 Myr if the slab descent rate is 50 mm yr^{-1}. The slab then shallows in dip (ii). Chronostratigraphic surfaces are shown for each 10 degree decrease in slab dip. In (iii), the age of slab at the ocean trench progressively decreases to 10 Ma, causing uplift (no erosion). After Gurnis (1992), reproduced with permission of American Association for the Advancement of Science.

of relatively buoyant mid-ocean ridges and plateaus (e.g. Peru trench).

One scenario is the subduction of progressively younger and more buoyant lithosphere as an ocean basin closes (Fig. 5.18). In this case, the negative dynamic topography (subsidence) at the initiation of steep subduction of an old plate would be restricted to a narrow zone close to the trench bordered by a bulge on the continental plate. Subsequent rapid shallowing of dip of the slab would drive the bulge towards the continental interior. As the ocean basin is eventually closed, the subduction of young oceanic lithosphere generates long-wavelength uplift, producing an extensive plateau in the retro-arc region.

Some of these features can be identified in the subduction history of the Farallon plate beneath North America (Conrad *et al.* 2004; Forte *et al.* 2007; Spasojevic *et al.* 2008) (Fig. 5.19). In the Tertiary, a very large tract of western USA was uplifted (e.g. Colorado Plateau) as the Farallon plate shallowed in dip and decreased in age (Cross 1986), leading to high gravitational potential energy and extensional collapse (Jones *et al.* 1996). A similar model has recently been applied to the tilting of Laurentia in the Ordovician to explain subsidence in the Michigan Basin (Coakley & Gurnis 1995) and to the entire North American craton during the Phanerozoic (Burgess & Gurnis 1995; Burgess *et al.* 1997). Different timings of subduction, different slab angles and ages, and different locations of subduction, are capable of producing the alternate periods of uplift and subsidence demonstrated in the six transgressive/regressive sequences (supersequences) of Sloss (1963) (Fig. 8.6).

The Farallon slab has also been used to model mantle convection backwards in time from the present-day tomography (Conrad & Gurnis 2003; Liu *et al.* 2008). These results clearly show the extent of subsidence in the Cretaceous Western Interior Seaway of west-central North America (Fig. 5.19).

A point that is rarely addressed but which is of major importance is that dynamic subsidence is transient rather than permanent. When the flow responsible for dynamic topography is removed, the continental interior should rebound to its non-dynamic position, at a rate determined by mantle viscosity. In the case of mantle plumes, igneous underplating of the crust causes a permanent isostatic subsidence, whereas dynamic uplift over the plume head is transient. Burgess and Gurnis (1995) correctly conclude that another mechanism must be present to allow long-term preservation of thick stratigraphic sequences in the continental interiors.

5.2.3 Dynamic topography associated with supercontinental assembly and dispersal

The history of continental migration is clearly marked by phases of continental aggregation into supercontinental assemblies, followed by break-up and dispersal before aggregation takes place once again (Anderson 1982; Kerr 1985) (§1.4.5). This recurring signal in the geological record is marked by collisional orogenesis during continental assembly, and extrusive volcanism and rifting during break-up (Condie 2004). Rodinia, Gondwana and Pangaea are all examples of

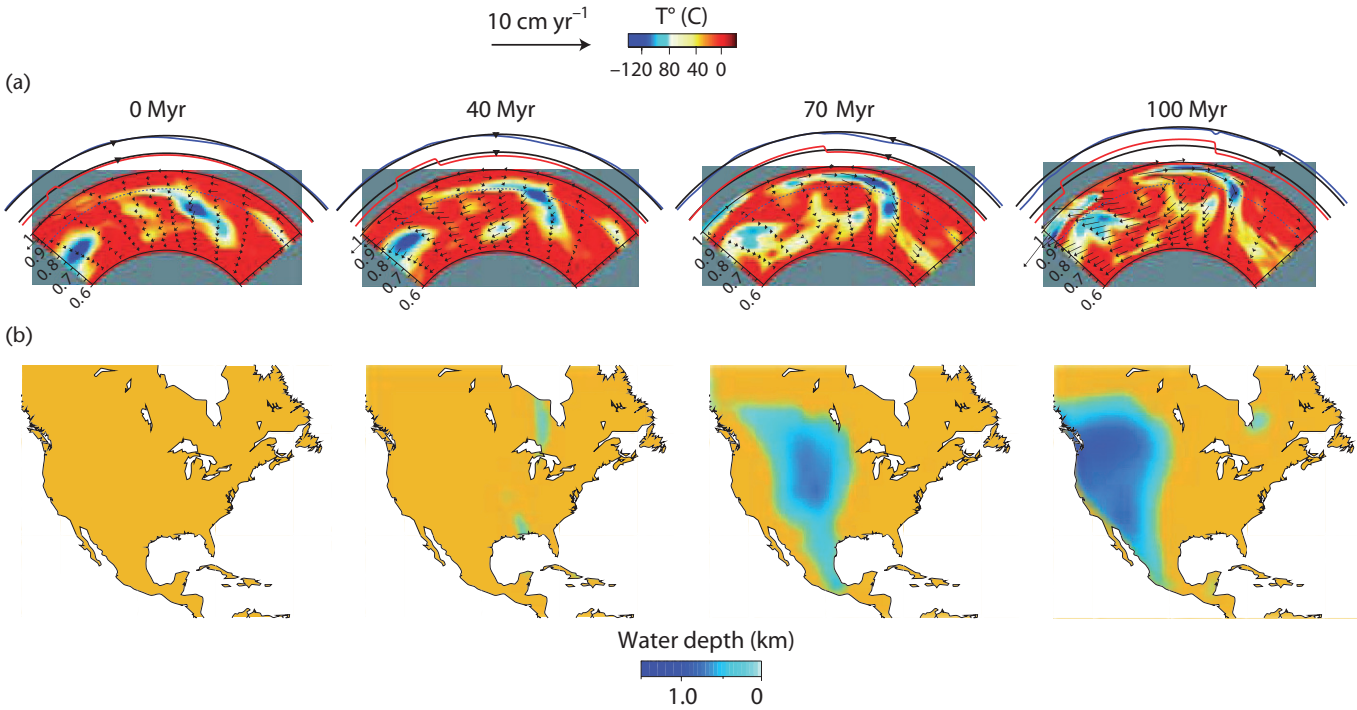

Fig. 5.19 (a) Cross-sections of the mantle (at 41°N) with velocity vectors (black) superimposed on the temperature field, due to subduction of the Farallon ocean slab from the left of the model and its passage beneath North America. The shallow subduction of the slab can be seen in the blue colours indicating cool temperatures. (b) Predicted continental flooding using an initially flat continent at 100 Ma and a eustatic sea-level correction from Haq & Al-Qahtani (2005). This model has a viscosity structure of 10^{20} Pa s for the upper mantle, 10^{21} Pa s for the transition zone and 1.5×10^{22} Pa s for the upper mantle. From Spasojevic *et al*. (2009), reproduced with permission of John Wiley & Sons, Inc.

supercontinental assemblies in the geological past. For example, the Laurentian (North American) plate broke away from a late Proterozoic Gondwanan supercontinent at about 575 Ma, then underwent accretions in the Late Devonian–Carboniferous (c.360 Ma) marking the initial assembly of the Pangaean supercontinent. By the Permian (c.250 Ma) Pangaea was a huge continental mass. In the Triassic (c.220 Ma) it started to split, with fragments dispersing rapidly in the Jurassic and Early Cretaceous. The time scale of the cycle above is of the order of 350 Myr. It should not escape the reader's attention that these aggregation-dispersal cycles roughly correspond with the first-order sea-level cycles of Vail *et al*. (1977a) and Haq *et al*. (1987) (see §5.4.3, §8.2.1).

Continents, and especially supercontinental assemblies, provide a different and more complex boundary condition for the heat loss of the Earth, since they introduce important lateral temperature variations across the continent–ocean boundary, and insulate the underlying mantle (Grigné *et al*. 2007). It is instructive to pause to speculate why the time scale of 300–400 Myr is characteristic of the 'supercontinental cycle' (Nance *et al*. 1988), since at present there is no theoretical basis for this regularity.

A number of time scales may be relevant. The diffusion time scale τ_κ can be written

$$\tau_\kappa = D^2/\kappa \qquad [5.10]$$

and represents the time it would take for a fluid layer of vertical dimension D to cool by conduction if convection ceased. With $\kappa = 10^{-6}\,\mathrm{m^2\,s^{-1}}$ and $D = 3000$ km, this conductive time scale is very large (many times the age of the Earth) and does not provide much information about the convective process. On the other hand, the convective time scale τ_c is given by

$$\tau_c = D/u = \tau_\kappa Ra^{-2/3} \qquad [5.11]$$

and represents the time it takes for fluid to cross the fluid layer of depth D at the convective velocity u. If $\mathbf{Ra} = 3 \times 10^6$, the convective time scale becomes 14 Myr, equivalent to a steady convective velocity of c.0.2 m yr^{-1}, whereas at $\mathbf{Ra} = 10^6$, $\tau_c = 130$ Myr and $v = 0.02$ m yr^{-1}, showing the strong dependency on Rayleigh number.

Instead, consider an insulating lid dominated by heat conduction to represent a slab of continental lithosphere above a fluid mantle (Fig. 5.20). The heat flux through the lid can be written

$$q = K_L \frac{T - T_0}{d} \qquad [5.12]$$

where K_L is the uniform thermal conductivity of the continental lid, and T and T_0 are the temperatures at the base and top of the lid of thickness d. If K is the thermal conductivity of the fluid layer of thickness h, and T_0 is set to zero, we obtain a thermal impedance term known as the Biot number

$$B = \frac{K_L}{K}\frac{h}{d} \qquad [5.13]$$

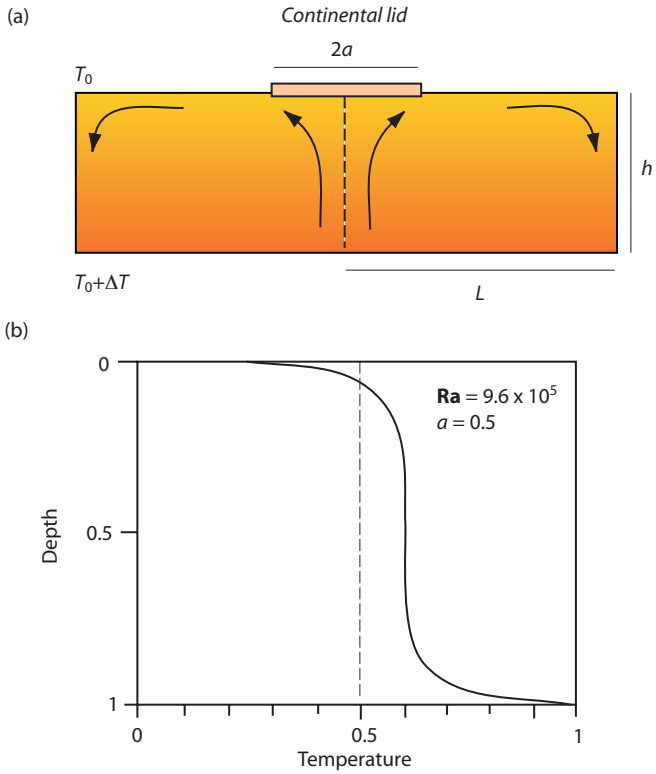

Fig. 5.20 (a) Geometrical parameters for convection beneath a supercontinent of half-width *a* acting as a lid conducting heat to the surface. There is no internal heating. Incubation of heat beneath the lid generates an upwelling, which feeds an elongate cell of width *L*. (b) Temperature profile beneath the continental lid from experimental work (Guillou & Jaupart 1995). Two dimensionless numbers characterise the flow: a Ra of c.10^6 and a dimensionless lid width of 0.5 ($2a/h$, where *a* is the half-width of the lid and *h* is the depth of the fluid layer). After Jaupart & Mareschal (2011, p. 268), reproduced with the permission of Cambridge University Press, 2002.

where **B** is small for a highly insulating lid. Note that the dimensionless number is the product of a dimensionless thermal conductivity and a dimensionless length scale. For the Earth K_L/K is slightly less than unity, and since d/h is approximately 10 under thick continental cores, **B** must be somewhat less than 10, which is relatively small. That is, the heat flux through the base of the thick continental lithosphere is small (c.10 mW m^{-2}) compared with the average heat flux through the oceanic plates driven by the convective cells in the mantle (100 mW m^{-2}). A wide insulating lid therefore has the effect of warming the mantle beneath it, but also of warming the entire interior of the Earth.

The presence of a wide, highly insulating lid also affects the circulation patterns in the mantle. For low continental extents (37% of the Earth's surface is covered with continents at the present day) of <40%, the flow pattern simply scales on the size of the continent or supercontinent (Lenardic & Moresi 1999; O'Neill *et al.* 2009). The fact that flood basalts are associated with supercontinental rifting and break-up suggests that the effects of the continental insulator are coupled in some way to processes in the deep mantle. It is possible that heating beneath the continental lid causes localisation of plumes, which transmit buoyancy-related viscous stresses, which in turn drives rifting, basin development and voluminous extrusive activity (Hill 1991; Courtillot *et al.* 2003). Alternatively, plumes may initiate from the lower thermal boundary layer at the core–mantle boundary in regions devoid of cold subducted slabs, which descend close to continental margins rather than under supercontinents (O'Neill *et al.* 2009). Heating beneath supercontinents could therefore be partly the result of the absence of the cooling effect of subduction, and partly the result of the relatively rapid advection of heat in plumes and/or relatively slow passive upward advection. The presence of the lid prevents this heat from escaping to the surface, as it does under the oceans.

The size of the supercontinent influences the flow structures in the heated mantle beneath. The sub-plate mantle may become organised into elongated convective cells, with aspect ratios determined by the width of the lid and by the Rayleigh number. When the Rayleigh number is greater than about 10^6, the simple cells become unstable, producing small-scale flow structures superimposed on the larger cell structure (Jaupart & Mareschal 2011, p. 268). This may be important for generating periodic uplift and subsidence of the continental surface (see §5.2.4 and §5.2.5).

Since the elongate large-scale cells beneath an insulating lid have a size dependent on the width of the insulating lid (Guillou & Jaupart 1995; Grigné *et al.* 2007; Phillips & Coltice 2010), the largest supercontinental assemblies are likely to have the greatest impact on the elevation of mean temperatures of the convecting fluid layer (Fig. 5.21). Small continents have difficulty in preventing the effects of cooling *via* subduction at their margins from affecting sub-plate temperatures. On the other hand, large supercontinents successfully prevent the ingress of subduction-related cooling. For very large continents, however, inefficient lateral advection of heat may cause drip-type instabilities to form in association with small-scale convection cells with a wavelength of <1000 km (O'Neill *et al.* 2009). Such instabilities may be important in individualising cratonic basin depocentres (see §5.4.2).

Gurnis (1988) conducted numerical experiments on the feedbacks between supercontinental assembly and dispersal, the geoid and mantle convection, the main results of which have been supported by experiments in a spherical geometry (Phillips & Bunge 2007). In experiments involving a single plate overlying a convecting mantle, a geodynamical cycle involves: (i) a phase of sub-plate heating over the upwelling, when the horizontal velocity of the plate is zero and the average horizontal stress is also zero. While the plate is stationary, the average temperature along its base rises (1 °C per 2.5 Myr for approximately 450 Myr gives a temperature increase of 180 °C) and its topography rises. (ii) Plate migration: as the sub-plate mantle is heated, the plate experiences significant tension. Its maximum topography corresponds to the time of maximum horizontal extensional stress. The plate moves rapidly off the hot upwelling, relaxing the extensional stresses and reducing its surface topography as it does so. (iii) Plate settling over a downwelling, when the average stress along its base becomes compressive. The topographic range experienced by the surface of the plate during this cycle is approximately 3 km. A plate located over an upwelling could accumulate sufficient extensional stresses to break, the two continental fragments dispersing rapidly towards adjacent downwellings, and eventually (150 Myr after

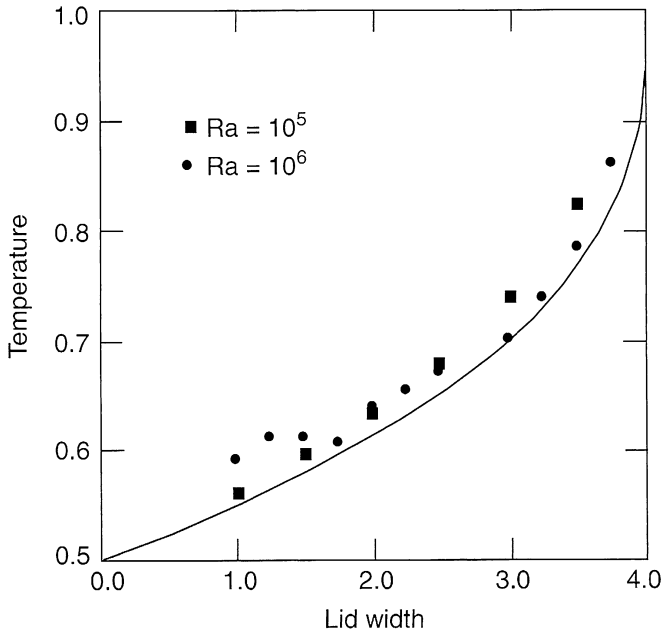

Fig. 5.21 Effect of lid width on the mean temperature of a convecting fluid layer, for two Rayleigh numbers of 10^5 and 10^6. Based on Grigné *et al.* 2007 (Jaupart & Mareschal 2011, p. 270), reproduced with the permission of Cambridge University Press, 2011.

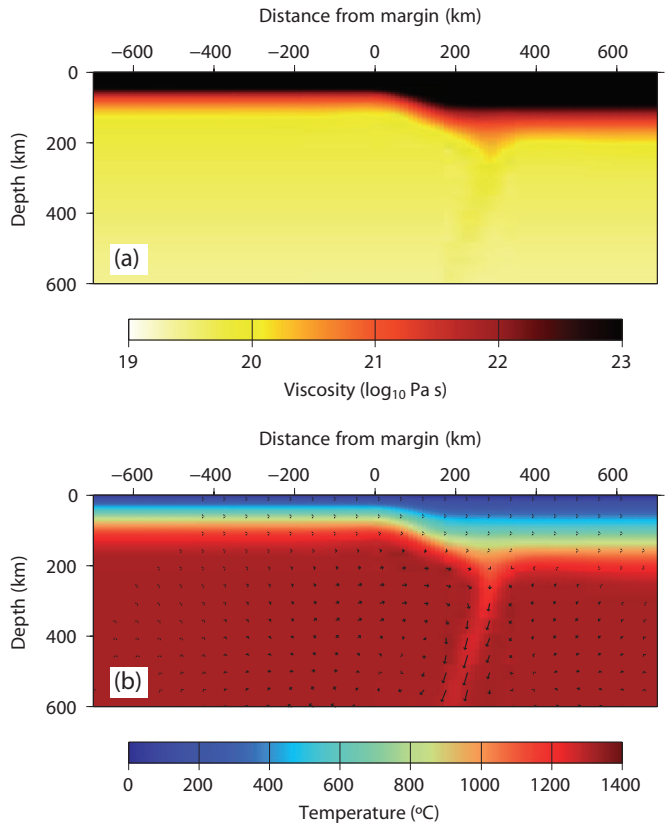

Fig. 5.22 Edge-driven convection or 'corner flow' associated with mantle circulation beneath a continental margin. The flow is generated after 40 Myr from a 100 km step in the thermally and compositionally defined lithosphere. (a) Viscosity, (b) temperature and flow vectors. Density is a function of temperature and melt depletion, and there is no pressure dependence. The model has an initial uniform density distribution. Density increases during evolution of the model by cooling of the ocean lithosphere. From John Armitage (pers. comm.).

break-up) colliding with each other again to form a new supercontinent. After about 450 Myr, the supercontinent has insulated the mantle for long enough to develop a new upwelling under the plate. Assembly of continental fragments and incubation of the mantle beneath the supercontinent is therefore very slow, whereas break-up and dispersal is relatively fast.

The time scale for a supercontinental cycle therefore depends primarily on the long time taken to incubate the sub-plate mantle sufficiently to inflate the supercontinent, cause break-up, and lead to the relatively rapid migration of continental fragments to adjacent geoid lows.

5.2.4 Dynamic topography associated with small-scale convection

It has been proposed (McKenzie 1967; Richter 1973; McKenzie *et al.* 1974) that there is a small scale of convection confined to the upper 650–700 km of mantle, but there is a lack of clear topographic expression and gravity field of the upwelling and downwelling limbs of such a convection system, or of lower lithosphere 'dripping' downwards to drive small-scale convection. It is possible, however, that small-scale convection may take place accompanying lithospheric stretching (Buck 1986; Keen & Boutilier 1995) or as an edge-driven effect at ocean–continental boundaries (Vogt 1991; King & Anderson 1998; Conrad *et al.* 2004). Edge-driven convection may be responsible for some LIPs situated close to continental margins, such as that of Victoria, Australia (King & Anderson 1995).

Steps in the base of the continental lithosphere, such as at the margins of cratons, and at the continental–ocean boundary (Fig. 5.22), may represent significant heterogeneities that interact with mantle flow, driving a pulsating secondary circulation with a downwelling fixed close to the ocean–continent boundary and an upward flow of hot mantle displaced about 600 km from the continental edge (Elder 1976; Vogt 1991). The Bermuda Rise is thought to be the seafloor bathymetric expression of such an upwelling, whereas the anomalously deep Nova Scotian margin of the northwestern Atlantic Ocean has been suggested to represent a cold downwelling of an edge-driven convection system (Conrad *et al.* 2004).

Pioneering models of edge-driven convection (King & Anderson 1995) required a shallow mantle beneath a continental lid that was hotter than under thinner lithosphere, as would occur under incubating supercontinents (Gurnis 1988). The small-scale edge-driven flow at a cratonic or continental margin interacts with the large-scale mantle flow. When this large-scale flow is small, the edge-driven effects stand out clearly, and model runs showed an increasing dominance of the edge-driven flow over time (King & Anderson 1998).

A second scenario is that the thick lithosphere is moving relative to the underlying upper mantle so that there is a shear between the two. If the mantle moves from the craton to the ocean relative to the lithosphere, that is, the flow experiences a negative step, the edge-driven flow maintains itself, but if the relative motion is in the opposite direction, that is the flow experiences a positive step, the edge-driven flow is lost in the larger-scale upper-mantle flow. Consequently, edge-driven circulation and its dynamic topography is likely to operate when continental assemblies incubate an underlying mantle that flows slowly towards the margins. Qualitatively, elevated bathymetry is expected in the oceanic lithosphere c.10^3 km from the continental edge, while the continental lithosphere adjacent to the continent–ocean boundary is expected to experience slow subsidence due to cold downwelling. Such edge-driven downwelling is expected to initiate during the period of continental inflation and extensional break-up. The negative dynamic topography associated with the downwelling under the continental or cratonic edge would take the form of low-angle ramp-like tilting towards the ocean, or sub-circular sags, depending on the three-dimensional nature of the edge-driven convection (for further discussion see §5.4.2).

Small-scale convection may also develop under continental lithosphere without the effect of a step at the continental edge (Petersen *et al*. 2010). The horizontal scale of the temperature variations modelled in the shallow mantle beneath the continental lithosphere is hundreds of kilometres, representing a considerably smaller length scale than expected for larger flow structures originating at the core–mantle boundary (Fig. 5.23). Fluctuations in the dynamic topogra-

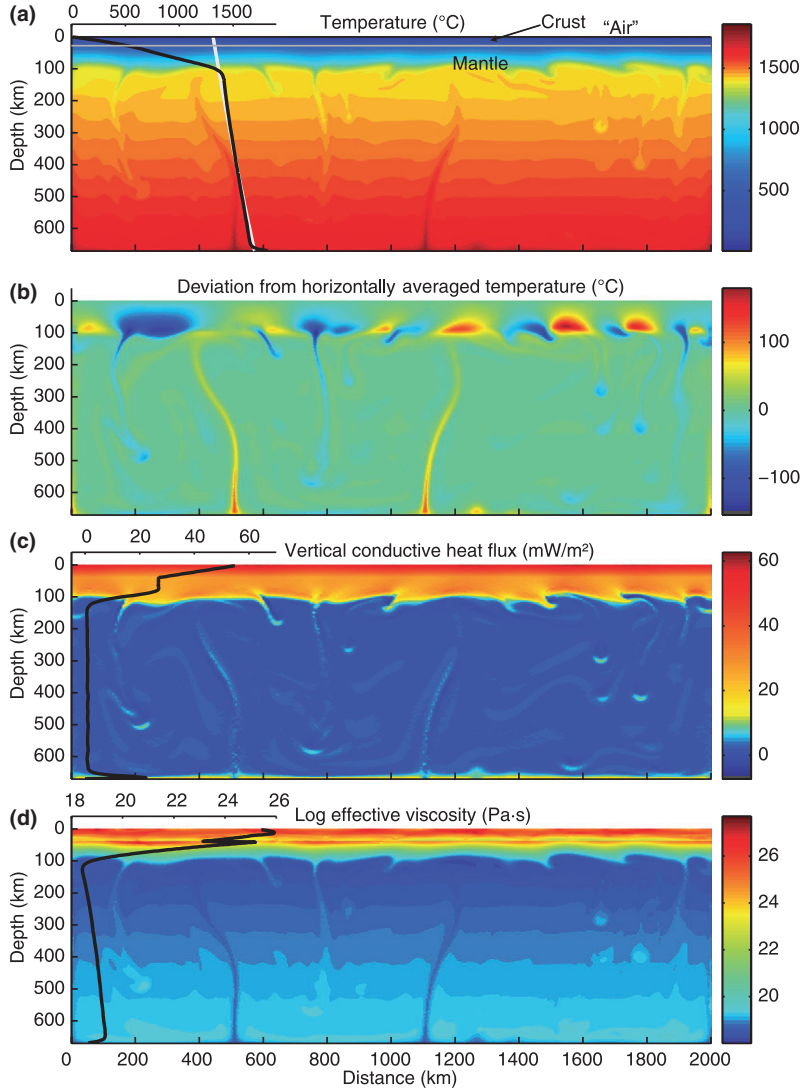

Fig. 5.23 Small-scale convection from a numerical convection model (Petersen *et al*. 2010). (a) Temperature. Black line shows averaged model geotherm, and grey line is the isentropic (adiabatic) profile for a potential temperature of 1315 °C. (b) Deviation from the horizontally average temperature. (c) Vertical conductive heat flux; black line is horizontal average. (d) Effective viscosity; black line is horizontal average. Note the development of small-scale instabilities, causing surface variations in heat flow and topography that may be important in the generation of stratigraphic sequences. Reproduced with permission of American Association for the Advancement of Science.

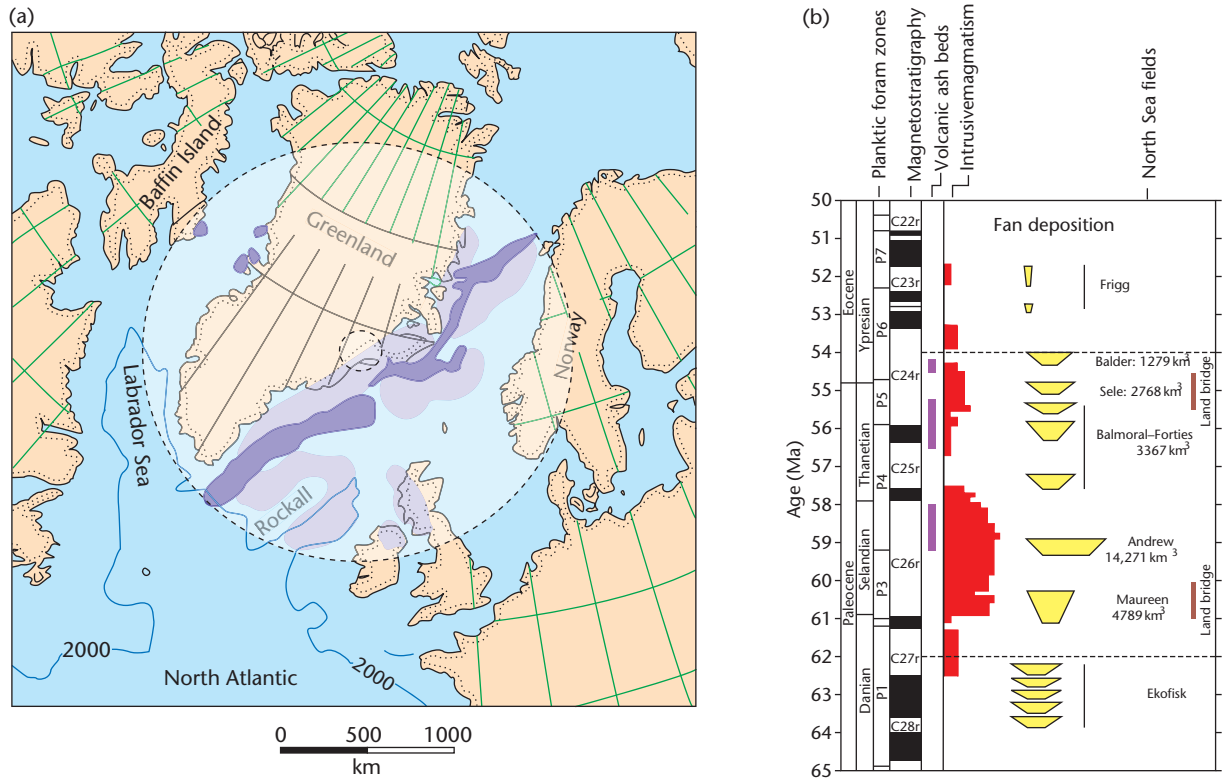

Fig. 5.24 (a) Reconstruction of the northern North Atlantic region just after the onset of ocean spreading (magnetic anomaly 23), showing the extent of the Iceland plume (White and McKenzie 1989; reproduced with permission of the American Geophysical Union). Solid shading shows position of extrusive volcanic rocks, and light shading shows extent of Early Cretaceous igneous activity. Uplift over the plume head, shown by circular area, can be recognised in thermochronological data such as apatite fission tracks. (b) Pulsing of the Iceland plume is thought to have caused episodic deposition of sands in the deep sea (White and Lovell 1997; reprinted by permission from Macmillan Publishers Ltd.). Periods of deep-sea fan deposition correspond to times of high levels of intrusive igneous activity.

phy of the continental surface of this length scale may explain the stratigraphic sequences of sedimentary basins.

5.2.5 Pulsing plumes

The periodic emplacement of sand beneath the deep waters of the North Sea during the Early Tertiary (White & Lovell 1997) (Fig. 5.24b) was interpreted as a result of pulsating activity of the nearby Iceland plume. Apart from causing variations over time in the volumes of erupted volcanic rocks (O'Connor *et al.* 2002), pulsating plumes might be expected to cause periodic phases of uplift of the seafloor (or continental surface), leading to the generation of erosional unconformities, tilting of sedimentary strata, and perhaps even to climate changes caused by the shallowing or occlusion of oceanographic gateways (Jones *et al.* 2001; Shaw-Champion *et al.* 2008; Hartley *et al.* 2011; Poore *et al.* 2011). Pulsing plumes may also cause phases of igneous underplating beneath the crust, resulting in relative uplift during intrusion followed by subsidence following crystallisation (McLennan & Lovell 2002).

The transmission of thermal pulses of the early Iceland plume is thought to have produced diachronous and transient relative uplift as they spread out from the main plume conduit (Rudge *et al.* 2008). The radially spreading mantle material is thought to flow in a channel of low viscosity beneath the plate, with instabilities giving rise to relatively rapid pulses of uplift and subsidence (Fig. 5.25). The dating of the transient uplift suggests that the uplift-subsidence motion (150–250 m – greater than can be accounted for by eustatic mechanisms) took place on the time scale of about 10^6 yr – smaller than the periods conventionally associated with convection, but similar to the periodicity of volcanic activity found in some hotspot chains (O'Connor *et al.* 2002).

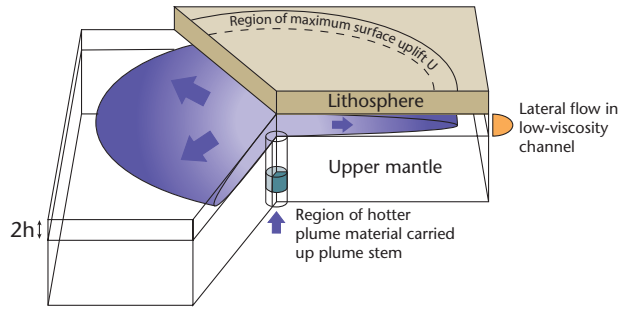

Fig. 5.25 Model for radial, channel-like flow associated with the impingement on the base of the lithosphere of a plume. After Rudge *et al.* (2008), reprinted with permission from Elsevier.

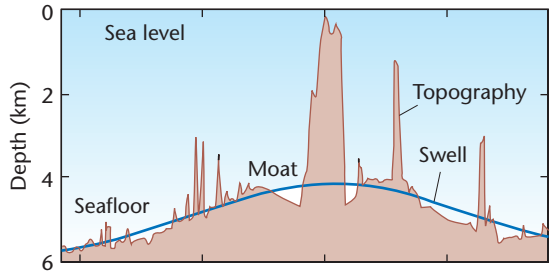

Fig. 5.26 Bathymetric profile of the Hawaiian Ridge at Oahu (after Watts 1978) showing that the hotspot swell is elevated about 2 km above the adjacent seafloor. Reproduced with permission of the American Geophysical Union.

The mechanisms that cause and control temporal variations in mantle plumes are not understood. Of the hypotheses that have been proposed, most have difficulty reproducing the correct frequency of multiple pulses, or need to invoke unrealistic excess temperatures and heat flows in the convecting upper mantle. It is currently uncertain whether variations in plume activity are related to changing fluxes of subducted cold material to the core–mantle boundary, to secondary instabilities within the plume conduit, or to interactions with phase transitions and rheological variations.

5.2.6 Hotspots, coldspots and wetspots

There is a smaller wavelength of thermal activity in the mantle compared to the very long wavelength (degree 2–10) of the geoid. This shorter wavelength pattern is shown by the spatial distribution of hotspots (Fig. 5.9) (see §5.1.5). Hotspots are at their most obvious in the ocean, where they are associated both with volcanism and strongly elevated topography. The Hawaiian Islands, Iceland and Canaries are all excellent examples. The recognition of hotspots on the continents is far more problematic. A key feature of hotspots is that they are assumed (perhaps incorrectly) to be fixed relative to a stationary reference frame in the underlying mantle, so absolute plate motion causes a hotspot track to be formed on the moving plate.

Initially, it is instructive to look at hotspot swells in the ocean (Table 5.1). Topographic uplifts over hotspots in the ocean are large, with swells elevated >1 km above the seafloor (Fig. 5.26). The topographic doming over a hotspot must be maintained by excess buoyancy. The buoyancy flux of eqn. [5.8] can be expressed in the alternative form (Davies 1988; Sleep 1990)

$$B = \Delta\rho W E u_p \qquad [5.14]$$

where $\Delta\rho$ is the density contrast of the uplift, WE is the cross-sectional area of the swell, and u_p is the plate velocity. The buoyancy fluxes of the Earth's present-day hotspots (Table 5.1) range over a factor of 20, with Hawaii at 8.7 Mg s^{-1} the largest. The average buoyancy flux for the 37 currently active hotspots is in the region of 1.35 Mg s^{-1}. It can immediately be appreciated that there is an inverse relationship between the cross-sectional area of the swell and the plate velocity for the same buoyancy flux from the mantle.

The Cape Verde swell typifies plume-related temperature anomalies and bathymetric relief (Courtney & White 1986) (Fig. 5.27). The best-fitting convection model to explain the temperature distribution involves a plume neck of 150 km diameter feeding a mushroom-like head of hot mantle material 1500 km across. The temperature anomaly in the plume head at the base of the plate is generally in the region of 100 °C, with the neck of the plume in excess of 300 °C above ambient asthenospheric temperatures. The centre of the Cape Verde swell is elevated by 1900 m relative to the normal oceanic depth; most of this relief can be attributed to dynamic uplift over the convecting plume head.

Geoid anomalies suggest that plume upwellings are spaced at about 2500–4000 km in the upper mantle beneath the oceans (McKenzie *et al.* 1980), but their distribution beneath the continental lithosphere is more speculative. The highspots associated with alkaline volcanism in north-central Africa, such as the Hoggar and Tibesti domes, may be related to activity in the underlying mantle (Thiessen *et al.* 1979; Sahagian 1980). Doming over hot plumes has also been interpreted as responsible for particular centrifugal paleodrainage patterns (Cox 1989) (§5.4.1), as well as for the eruption of vast piles of basalts (§5.3.1, §5.3.2).

Hotspots should also produce swells on the continental lithosphere. Taking the globally 'typical' hotspot ($B = 1.35$ Mg s^{-1}) and a continental plate ($\Delta\rho = 2700$ kg m^{-3}) with a track velocity of 20 mm yr^{-1}, the cross-sectional area of an average topographic dome is about 800 km^2. For a dome elevated at 1 km above the regional elevation, we would expect a width of c.1000 km. For a fast-moving plate (say 100 mm yr^{-1}), the cross-sectional area reduces to just 160 km^2 for the same buoyancy flux. Since slow-moving plates are likely to have better developed hotspot swells than fast-moving plates, hotspot swells should be more significant and more easily recognised at times of continental assembly before rapid plate dispersal.

Fluid dynamical work (Griffiths & Campbell 1990; Hill 1991) suggests that low-viscosity plumes may initiate from within the Earth and ascend as a spherical pocket of fluid (plume head) fed by a pipe-like conduit (plume tail) continuously supplying buoyant, hot material to the head region (Fig. 5.28). It is likely that enlargement of the plume occurs by the entrainment of material heated by the ascent of the plume from the core–mantle boundary. Flood basalt provinces have been interpreted as originating through the melting of the heads of newly started plumes, whereas oceanic island chains represent the tracks of the relatively long-lived plume tails as the plate migrates over the mantle.

Fluid dynamical experiments also suggest that the diameter of a new plume head varies according to the volume flux and temperature excess of the source material provided to the plume head, and the thermal and viscosity properties of the lower mantle into which the plume starts to ascend (Griffiths & Campbell 1990). The plume head then grows by entrainment as it ascends through the mantle, so that the plume head diameter grows as a function of the distance travelled. By the time the plume head has penetrated into the upper mantle it should have cooled to only 100–200 °C above the ambient temperature.

Upon nearing the surface of the Earth, the plume head spreads out into a disc of hot material with positive buoyancy (Fig. 5.28a). This produces a dynamic surface uplift. The scaling of laboratory experiments suggests that the timing and magnitude of the surface uplift depend strongly on the viscosity of the upper mantle. The results from laboratory experiments in which a plume head is sourced from the core–mantle boundary with a buoyancy flux of 3×10^4 N s^{-1} and a source temperature excess of 300 °C, lower mantle dynamic viscosity of 10^{22} Pa s (kinematic viscosity of 2.5×10^{18} m^2 s^{-1}) ascending into an upper mantle with a viscosity of 3×10^{20} Pa s, is shown in Fig. 5.28b. The surface is initially weakly uplifted while the plume head

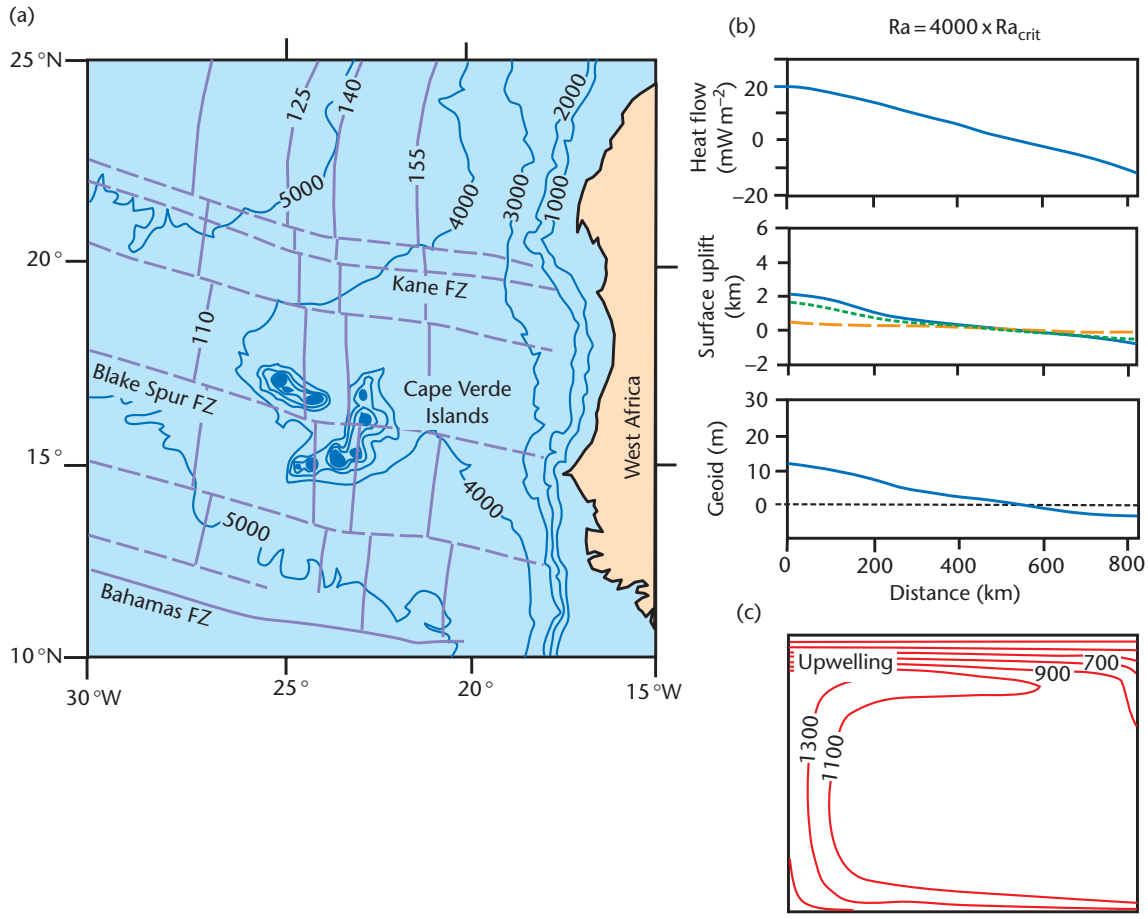

Fig. 5.27 Cape Verde hotspot. (a) Bathymetric map (in m) of the Cape Verde Rise, with isochrons in Ma. Fracture zones are shown in dashed lines. (b) Heat flow, surface uplift and the geoid for a convection cell at 4000 times the critical Rayleigh number for convection. The total uplift is shown as a conductive component (dashed) and a convective component (dotted). (c) Temperature distribution responsible for the results shown in (b). After Courtney & White (1986), reproduced with permission of Oxford University Press.

is entirely within the lower mantle (–25 Myr). When the plume head enters the low-viscosity zone of the upper mantle (–3 Myr) the surface uplift takes place rapidly, reaching a maximum elevation of 600 m after further ascent to just beneath the lithosphere. At this stage the plume head has a diameter of 1300 km. A number of factors may increase the maximum elevation of the topographic dome: (i) penetration of the hot plume into the cold lithosphere; and (ii) a volume increase caused by melting. The release of large amounts of basalts by melting of the plume can only take place once the plume head has reached shallow depths. It should be noticed that this is only possible a number of millions of years after the maximum surface uplift. The development of smaller-scale gravitational instabilities over the cap of the plume as cold, dense material is squeezed between the ascending plume head and the Earth's surface may facilitate the last-stage ascent of the plume and produce the high surface uplifts seen today in locations such as East Africa, and the large outpourings of basalts in the geological past, such as the Siberian and Deccan (India) Traps (Fig. 5.8).

Hotspot swells in the oceans are well documented. We might also expect topographic uplift of the continents over sub-lithospheric upwellings. Such uplifts are likely to be of the order of 1 km in height and perhaps 1000 km in width. The domes of Africa, such as the Hoggar of the Saharan region, and the Bié and Namibian domes of southwest Africa (Al-Hajri *et al.* 2010), are good candidates for uplift over upwellings. Over geological time, all the continents must have passed over mantle upwellings, leaving hotspot tracks. Some parts of continents must have a veritable criss-cross pattern of hotspot tracks (Morgan 1983). Within a band of approximately 10^3 km width, the continental surface should be transiently elevated, leading to erosion and the development of regional unconformities. Such unconformities would be recognisable long after the transient dynamic uplift has ceased. If we ignore flexural uplift due to mountain building (Chapter 4), and dynamic topography related to plate subduction (§5.2.2) and supercontinental assembly (§5.2.3), involvement in hotspot uplift may be a major cause for erosional unconformities in cratonic sedimentary sequences.

If there are upwellings beneath continents, we should also expect there to be downwellings, which would be cold and characterised by negative dynamic topography. The Congo Basin may be situated over one such downwelling (Hartley & Allen 1994; Downey & Gurnis 2009; Crosby *et al.* 2010, but compare Buiter *et al.* 2011). It is situated adjacent to the East African upwelling. The fact that many

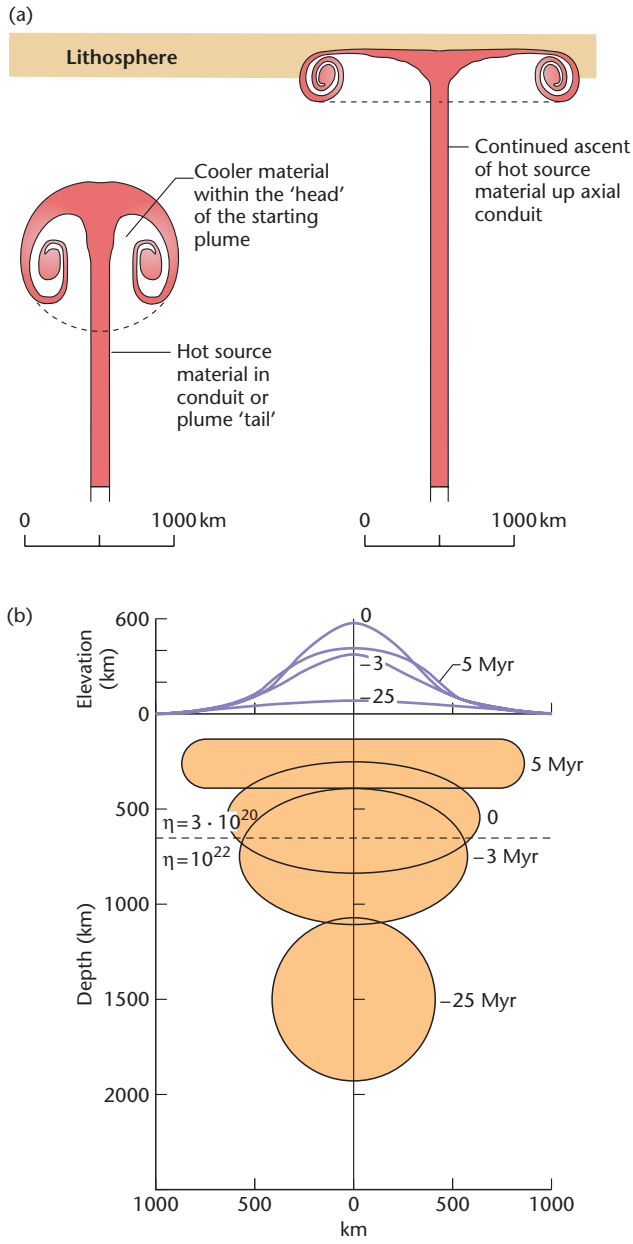

Fig. 5.28 (a) Schematic diagram of the ascent of a plume through the mantle and its mushrooming into a disc beneath the lithosphere, with darker shading indicating higher temperatures, after Hill (1991) and reprinted with permission from Elsevier. (b) The dimensions of a starting plume together with the predicted uplift, based on laboratory experiments. During the lateral spreading of the head, the input of material from the source is discontinued, simulating the carrying away of the head from the source region by plate motion. After Griffiths & Campbell (1990), reproduced with permission of the American Geophysical Union.

sedimentary basins have sedimentary sequences deposited over long periods of time raises the possibility that small-scale convection systems are pinned to the lithospheric plates (see §5.2.4). If so, these convection systems would have upwellings that do not move significantly relative to the plate, in contrast to the well-developed hotspot tracks caused by migration of a plate over a quasi-stationary system of mantle upwellings.

Hotspots and highspots should of course be important source areas of erosional detritus. Peripheral uplifts around a sedimentary basin may feed the basin with sediment and load the lithosphere. In this sense, some cratonic basins may be more passive receptacles for the erosional detritus of peripheral or annular uplifts than areas with strong mechanical subsidence (see Sahagian 1993 for a similar view).

The presence of volatiles reduces the solidus for mantle rocks and therefore promotes melt generation, and hydration decreases density, generating buoyancy. Consequently, topographically elevated volcanic hotspots may reflect mantle wetspots rather than plume heads. A wetspot might result from the subduction of oceanic crust, for example. However, volcanic seamount chains such as Hawaii have persisted for 100 Myr, so there is a problem in the required volume of water-rich mantle rock.

It has also been suggested that the buoyancy of topographically elevated hotspots might be a compositional effect caused by depletion in iron after melt extraction (Morgan *et al.* 1995). It is unlikely, however, that this effect can explain the entire buoyancy represented by the topographic swell.

5.3 Mantle dynamics and magmatic activity

Igneous activity is a common feature of some continental rifts and passive margins at the point of break-up. Igneous activity is caused by adiabatic decompression due to one or a combination of lithospheric stretching, elevated asthenospheric temperatures and presence of volatiles. Hot plumes derived from the core–mantle boundary have a profound effect on asthenospheric temperatures, melt generation by adiabatic decompression and surface uplift. Plume heads occupy areas of the asthenosphere generally 1000–2000 km across with temperature anomalies of 100–200 °C, and in the oceans are responsible for bathymetric swells 1–2 km above the surrounding seafloor. The elevation of sub-lithospheric temperatures over a mantle plume may generate large amounts of melting and the upward migration of melts to form igneous underplates and extrusive basalts. Transient surface uplift is caused by the dynamic effects of hot asthenospheric flow, whereas permanent uplift results from igneous underplating of the crust. Consequently, volcanically active passive margins and continental rifts stand elevated topographically compared to non-volcanic equivalents. The amount of melt generated and its composition is related to the plate thickness, excess temperature, stretch factor and percentage of volatiles.

It is beyond doubt that some regions of continental stretching are unrelated to any 'active' thermal processes. However, in other instances, continental stretching and break-up are associated with voluminous basaltic volcanism, as in the Deccan of India, the Karoo of southern Africa and the Parana of South America. Magmatically active rifts and continental margins are commonly associated with anomalously high temperatures in the asthenosphere caused by the presence of mantle plumes (White & McKenzie 1989).

The long chains of volcanic islands (e.g. Hawaiian-Emperor seamount chain) and bathymetric swells in the oceans are associated with the eruption of extensive basalts whose geochemistry indicates that they originate by melting of mantle elevated above the normal temperature of the asthenosphere. Such high temperatures are thought to be due to the ascent of hot material from the lower thermal boundary layer at the base of the mantle. Two sorts of uplift pattern and igneous activity should result from plume activity,

depending on whether the lithosphere overlies a plume head or plume tail. Plume head regions should be areally extensive and equant (1500 km to 2500 km across), giving rise to LIPs, whereas plume tail provinces should be narrow (<300 km wide) and linear, that is, they should be hotspot tracks.

5.3.1 Melt generation during continental extension

Igneous activity in sedimentary basins is diagnostic of basin-forming mechanisms. In the reference uniform stretching model of McKenzie (1978a), no melts are generated because the geotherm does not intersect the solidus for crustal and mantle materials. However, it is well known that rift provinces are associated with minor (e.g. Western Rift, Africa, North Sea) to major (Eastern Rift, Africa, Rio Grande) volcanism. Most importantly, continental break-up at high values of stretching is commonly associated with vast outpourings of flood basalts, indicating major melting of the asthenosphere by adiabatic decompression. Melts liberated by decompression are assumed to separate from their residue and to travel upwards to either be erupted at the surface, or to be emplaced as igneous bodies in the crust. McKenzie and Bickle (1988) showed how the amount of melt generated depends on the potential temperature of the asthenosphere – defined as the temperature the asthenosphere would have if brought to the surface adiabatically without melting – and the amount of stretching (Fig. 5.29). For example, if a 100 km-thick lithosphere is stretched by a factor of 2, we would expect a melt thickness of about 2 km for a potential temperature of 1400 °C. At higher values of stretching ($\beta = 5$), we would expect a melt thickness of 10 km for the same potential temperature. The normal potential temperature of the asthenosphere is 1280 ± 30 °C, so the examples above refer to an excess temperature of the order of 100 °C attributable to plume activity.

The conditions at the site of partial melting are reflected in the composition of the erupted basalts. Stretching at infinitely high values at a normal asthenospheric potential temperature of 1280 °C produces melt with the composition of a mid-ocean ridge basalt (MORB). However, increasing the potential temperature to 1480 °C causes an increase in MgO and a decrease in Na_2O. Consequently, we would anticipate the generation of first alkali basalts and then tholeiitic basalts as stretching increases over an asthenosphere with a potential temperature of 1480 °C.

The presence of a hot asthenosphere affects the subsidence experienced at the Earth's surface caused by lithospheric stretching. This is mainly caused by two effects: the addition of igneous bodies beneath the crust (see below), and the dynamic uplift from the mantle plume.

The density of igneous rock generated by adiabatic decompression of the mantle depends on the potential temperature at the site of partial melting, and ranges between 2990 and 3070 kg m^{-3} (at a depth of 10 km) for potential temperatures of 1280 °C and 1480 °C respectively. This range of density is mid-way between the density of the continental crust and the density of the mantle, so there is a strong likelihood that melts will be trapped and underplated beneath the crust. Since these igneous additions replace lithospheric mantle (density 3300 kg m^{-3}), the net effect is uplift relative to the depth expected from uniform stretching of the lithosphere without magmatic activity (Appendix 27).

Assuming Airy isostasy, the amount of underplating X required to generate an amount of surface uplift U can be found by balancing

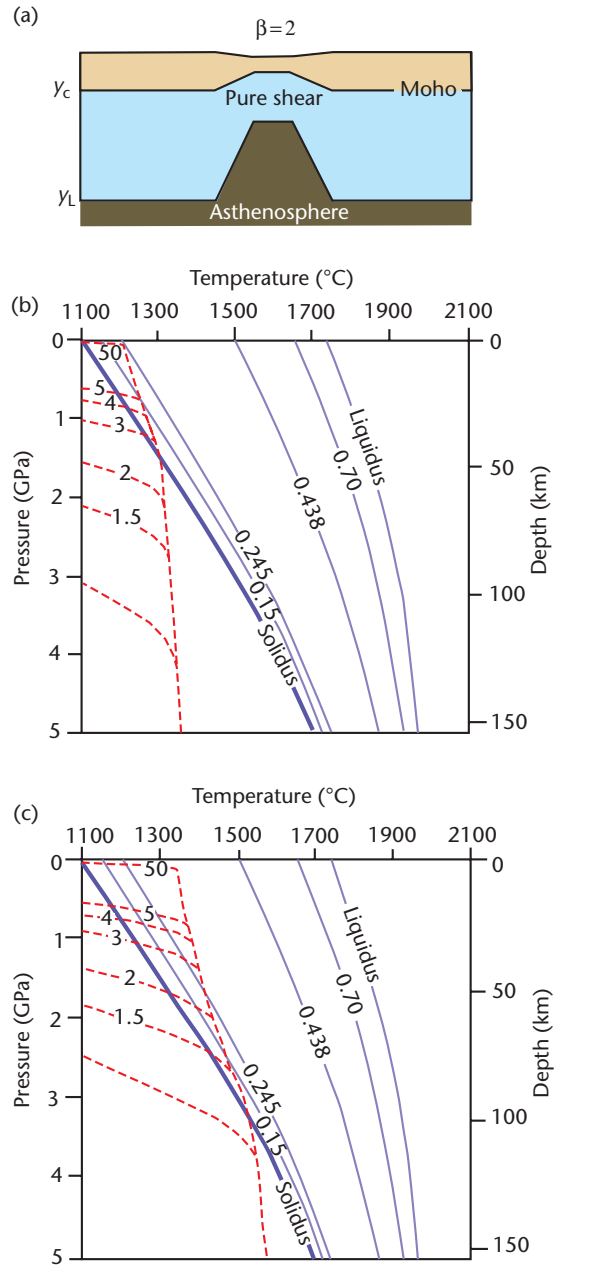

Fig. 5.29 Melt generation by adiabatic decompression during pure shear extension, based on McKenzie & Bickle (1988), White & McKenzie (1989) and Latin & White (1990). (a) Uniform stretching of the lithosphere by a stretch factor of 2. (b) Adiabatic upwelling due to stretching at different values of β from 1.5 to 50. Potential temperature of the asthenosphere 1280 °C, mechanical boundary layer thickness of 100 km, kinematic viscosity 4×10^{15} m^2 s^{-1}. Curves between the liquidus and the solidus show the melt fraction by weight. Only small amounts of melt can be produced at high values of stretching. (c) As for (b), but with a potential temperature of 1480 °C, showing that large amounts of melt can be liberated at relatively low values of the stretch factor.

two lithospheric columns. In the undisturbed column, crust of thickness y_c and density ρ_c occurs within a lithosphere of thickness y_L and subcrustal density ρ_m. In the underplated lithospheric column, crust of the same thickness is underlain by a layer of basaltic underplate with thickness X and density ρ_x. The total thickness of this lithospheric column is y_L plus the surface uplift U.

Balancing the pressures at a depth of compensation at the base of the lithosphere yields

$$U = X\left(1 - \frac{\rho_x}{\rho_m}\right) \qquad [5.15]$$

The density of the mantle lithosphere can be taken as 3300 kg m^{-3} and the density of the basaltic underplate as 3000 kg m^{-3}. The rock uplift for an underplate thickness of 5 km is therefore 455 m, or approximately one tenth of the underplate thickness. This is also the surface uplift without any erosion. We can incorporate erosion in the simplest way as follows (Brodie & White 1994). Consider a piece of lithosphere underplated with basalt of thickness X that is eroded so that the surface elevation change is zero (Fig. A27.1). The crust therefore has a thickness of y_c minus the denudation D. We can once again perform an isostatic balance, giving

$$D = X\left(\frac{\rho_m - \rho_x}{\rho_m - \rho_c}\right) \qquad [5.16]$$

where D is the total denudation of crust caused by the emplacement of a basaltic underplate of thickness X. The total denudation for an underplate thickness of 5 km if there is no change in the surface elevation is 2.5 km, if crustal rocks of density 2700 kg m^{-3} are eroded. We therefore have the maximum erosion case and the no-erosion case. Reality is probably in between. Clearly, magmatic underplating can have significant effects on surface uplift and on the delivery of erosional products to neighbouring sedimentary basins (White & Lovell 1997). The uplift caused by magmatic underplating is permanent.

The circulation in the mantle plume maintains anomalously high temperatures that cause a dynamic uplift, as described above. The combined effect of underplating and dynamic support is to elevate the continental plate to sea level or above during the rifting process for excess asthenospheric temperatures of 100–150 °C. This is entirely supported by the observation that the basalts erupted at rifted continental margins are commonly subaerial rather than submarine, and flow for large distances downslope to produce extensive flood basalt provinces.

5.3.2 Large igneous provinces

It is known that hotspot tracks emerge from LIPs, or flood basalt provinces (Morgan 1981). The tracks are marked by volcanoes with an age progression along the chain, highly suggestive of the relative movement of the oceanic plate across a plume tail. The end of the track is a currently active volcano. Correspondingly, large equant igneous provinces are interpreted as the result of impingement of a plume head on the base of the lithosphere. The largest submarine flood basalt province is the Ontong Java Plateau east of Papua New Guinea, whereas the Siberian traps of northwestern Russia, the Karoo of southern Africa, and the Parana of South America are celebrated continental flood basalt provinces from the geological record (Duncan & Richards 1991).

5.3.3 The northern North Atlantic and the Iceland plume

The northern Atlantic contains extensive basalts covering c.500 × 10^3 km^2 on both sides of the ocean in Greenland and in northwest Britain, Ireland and the Faroes (Fig. 5.24). The basalts range from 52–63 Ma in age, with a main eruption phase at 59 Ma (Mussett *et al.* 1988). The thermal anomaly responsible for these igneous provinces is now located beneath Iceland. The Iceland region continues to be dynamically supported by the underlying plume over an area of anomalously shallow seafloor with a radius of 1000 km.

In the subsurface seismic record, extrusive basalt sheets can be recognised as seaward-dipping reflectors along both the east Greenland and Rockall–Faroes–Norwegian margin. Volumetrically smaller basaltic volcanism can be seen in onshore exposures such as the Tertiary Igneous province of northwest Scotland and northeast Ireland. Thick (<8 km) prisms of accreted igneous rocks with seismic velocities >7.2 km s^{-1} have been imaged across the Hatton Bank and Voring Plateau beneath thinned continental crust, most likely representing underplated igneous rocks. White and McKenzie (1989) estimate the combined underplate and extrusive basalt volume as <10^7 km^3.

The Icelandic plume has been identified as the 'smoking gun' for the widespread surface uplift of the North Atlantic area in the Early Tertiary (Paleocene). The regional surface uplift caused by underplating and dynamic support is thought to have promoted high rates of denudation and transport of particulate load into the deep-sea environments of the North Sea and NW Atlantic margin basins. High rates of denudation in large areas of northwestern Europe during the Early Tertiary can be inferred from apatite fission track analysis (papers in Doré *et al.* 2002). In the neighbouring sedimentary basins, such as the Faroes–Shetland Basin and the Rockall–Porcupine troughs, sandstones were episodically delivered from this exhuming continental landmass. White and Lovell (1997) suggested that the main pulses of submarine fan deposition correspond to the main pulses of magmatic activity during the time period 62 to 54 Ma.

5.3.4 The Afar region, Ethiopia

The Afar region of northeast Africa is currently undergoing extension, accompanied by voluminous intrusive and extrusive magmatism. It illustrates the magmatism associated with continental break-up and the transition to a new ocean basin, during continental rifting (Ebinger & Casey 2001). The uppermost mantle beneath the Horn of Africa (to a depth of 400 km) is seismically (P- and S-waves) slow (7.4–7.5 km s^{-1}) (Fig. 5.30), suggesting that the mantle is hot and most likely subject to partial melting. It has been suggested that the mantle beneath Ethiopia is the hottest on Earth (Bastow *et al.* 2008). One view is that the Ethiopian region is the location of a plume stem originating from a northward continuation of the African superplume (Furman *et al.* 2006) – a deep, long-lived, thermal structure with a footprint on the core–mantle boundary of 2000 × 4000 km and a height of 2000 km. An alternative view is that it is part of a single large plume centred on Turkana (Ebinger & Sleep 1998), and a further possibility is of two plumes rising beneath southern Ethiopia and Afar (Rogers *et al.* 2000).

A characteristic feature of continental rift provinces overlying hot mantle is that a large (~80%) part of the extension is achieved by the

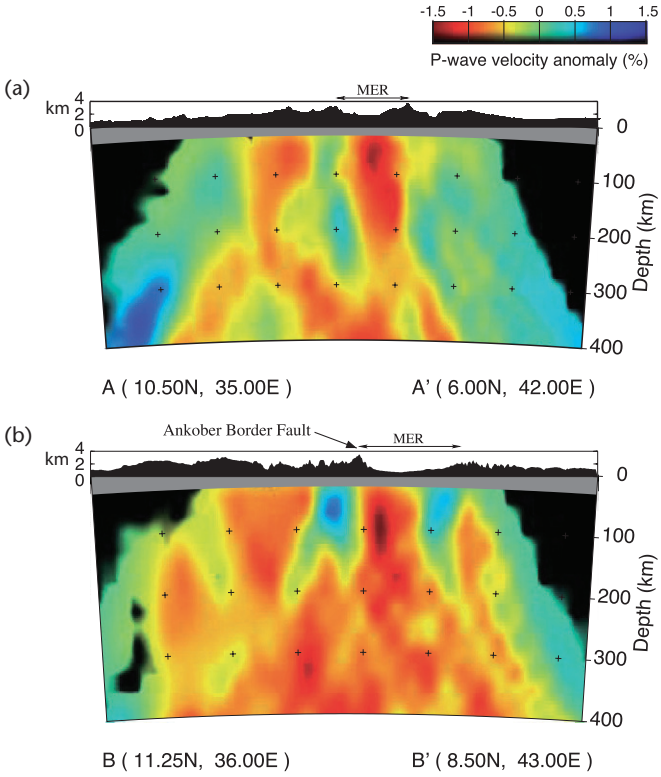

Fig. 5.30 Vertical cross-sections of the P-wave velocity model, with contours in P-wave velocity anomaly (%), for (a) the continental rifting part of the Ethiopian region, and (b) the region of transition to ocean crust towards Afar. The low-velocity zone extends from 75–400 km depth and is thought to be the northward continuation of the African superplume. The very slow velocities are thought to be due to partial melting in the upper mantle. The Main Ethiopian Rift (MER) is situated towards the eastern flank of the low-velocity structure, not above its centre, suggesting that pre-existing tectonic structures are important in localising melt migration at the base of the lithosphere. From Bastow *et al*. (2008), reproduced with permission of John Wiley & Sons, Inc.

intrusion of dykes, as occurs below the Baikal rift (Thybo & Nielsen 2009). This means that stretch factors are relatively low, which affects the timing and volume of decompression melts generated by thinning during advanced stages of plate break-up. Magma intrusion also reduces plate strength, thereby causing later localisation of stretching. The Main Ethiopian Rift is consequently displaced towards its eastern edge from the locus of the underlying low-velocity zone.

The final stretching leading to a new ocean basin caused voluminous (2 km thick) basaltic volcanism due to decompression melting of the asthenosphere at 29–31 Ma. This is just prior to, or at the same time as the onset of rifting in the Red Sea and Gulf of Aden. These flood basalts of the NW Plateau directly overlie the low-velocity zone in the upper mantle. Active volcanism continues to the present day in the Afar Depression and parts of the Main Ethiopian Rift. Low-temperature thermochronometry suggests that Ethiopia experienced surface uplift at 30–20 Ma. Extension in the Main Ethiopian Rift started at ~20 Ma in the south of the region, but migrated to the north at ~10 Ma. The coincidence of the onset of topographic uplift and the onset of extrusive volcanism at 30 Ma suggest that they both relate to the arrival of a hot mantle flow structure beneath the area, though whether it was a plume head (Griffiths & Campbell 1990; Hill 1991) followed by a narrow conduit or tail, is unknown. Early dyking controlled the orientation of later border faults, which accommodated most slip some millions of years later.

5.4 Mantle dynamics and basin development

Mantle dynamics influence basin development in a number of possible ways. Principally, mantle processes control dynamic topography (§5.2), which has an important impact on the location and elevation of source regions for sediment and on the location and rate of subsidence of sedimentary basins. However, extracting the component of dynamic topography from the total topographic signal of the surface of the Earth and from its sedimentary archive is challenging. The most promising situations are areas where other basin-forming mechanisms are absent or subdued, such as in continental interiors. Cratonic basins (§5.4.2) therefore offer the possibility of inverting mantle processes from the stratigraphic record.

Topography supported by convective flow in the mantle occurs at different wavelengths and amplitudes. The dynamic topography due to the African superplume (Nyblade & Robinson 1994) is approximately 500 m over a large part of the African continent, whereas the dynamic topography related to the convective cells responsible for hotspots is likely to be 0.5–1 km over a much shorter wavelength of 500–1000 km. In addition, a number of domal uplifts occur close to the ocean–continent transition in western Africa, such as the Namibian dome (Al-Hajri *et al*. 2010).

5.4.1 Topography, denudation and river drainage

It is a challenging problem to estimate the dynamic topography of the continental surface in the geological past. One approach is to map the stratigraphic gaps of unconformities attributable to dynamic support, and to convert denudation estimates to amounts of topographic uplift. Phases of uplift also correspond to pulses of increased sediment delivery to offshore sedimentary depocentres (Walford *et al*. 2005). This procedure has been carried out, for example, in the late Cenozoic domal uplifts in southwestern Africa (Al-Hajri *et al*. 2010) (Fig. 5.31). Whereas a phase of Oligocene uplift is attributed to the initiation of the African superplume, a Pliocene unconformity suggests the rapid emergence of a number of smaller domes around the western perimeter of the superplume.

Surface uplift of the continental surface affects the course of river systems draining the elevated region. Centrifugal drainage patterns may develop over domal uplifts (Cox 1989). River long profiles potentially contain information about the uplift history experienced by the drainage area (Roberts & White 2009; Pritchard *et al*. 2009), since erosional landscapes respond to relative uplift by the upstream passage of a wave of erosion recognised by a knickzone (Fig. 5.32) (Appendix 47). When applied to African examples (Fig. 5.31), where topography is expected to reflect convective circulation (Burke & Gunnell 2008), a coherent picture of surface uplift, denudation and sediment supply to the ocean is obtained. In the magmatic domes of Hoggar and Tibesti of Saharan Africa, and the amagmatic domes of Bié, Namibia and South Africa, uplift started 30–40 millions of years ago. A further application to the rivers of the Colorado Plateau

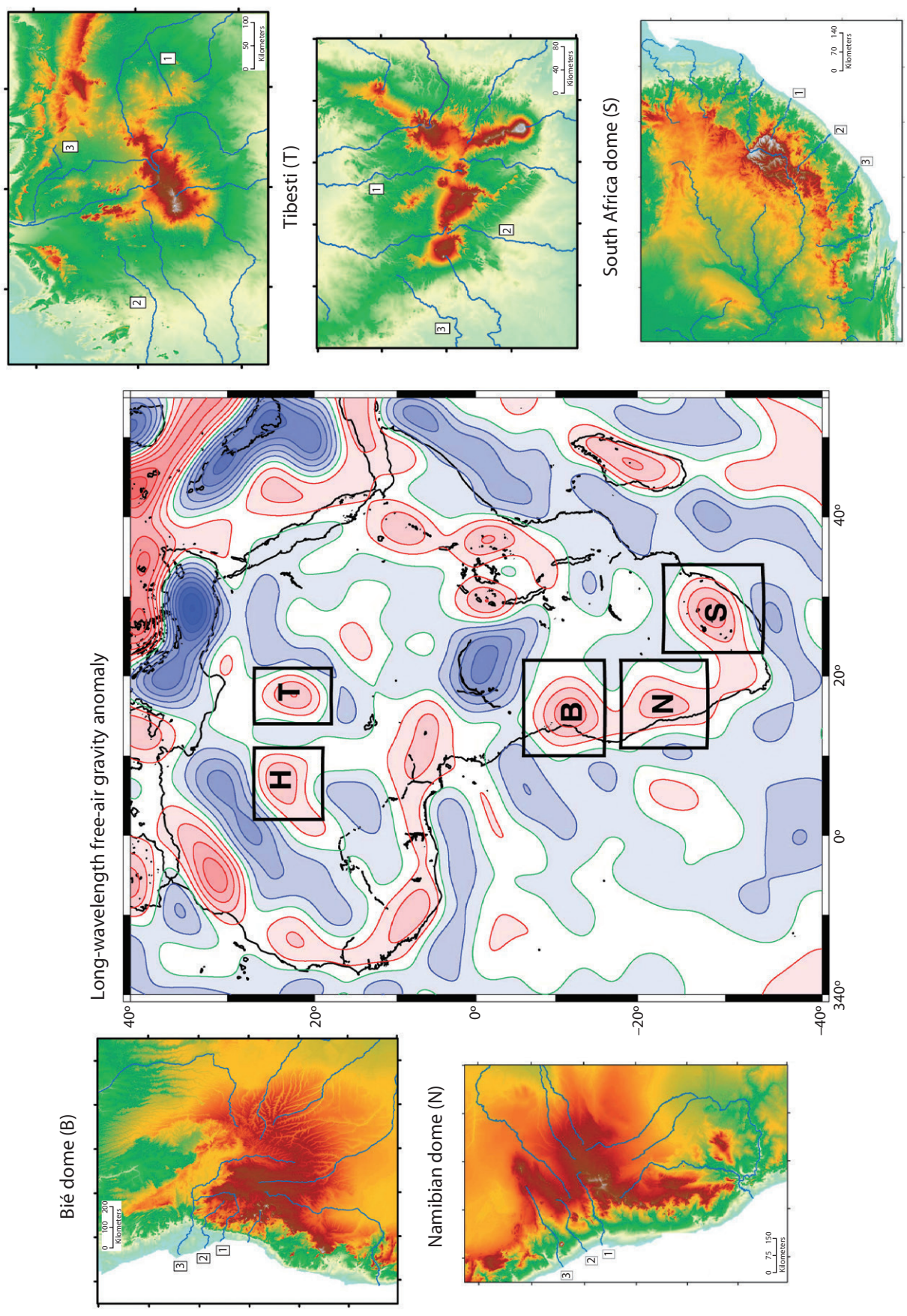

Fig. 5.31 Long-wavelength free-air gravity map of Africa, from Roberts & White (2010), showing positive (red) and negative (blue) anomalies, contoured at 5 mGal. The long-wavelength gravity anomalies may represent convective circulation beneath the lithosphere. Boxed positive anomalies are topographic domes where rivers have been analysed in order to estimate the timing of uplift events from knickpoints. H, Hoggar; T, Tibesti; B, Bié dome; N, Namibian dome; S, South Africa dome. Rivers whose long profiles were used are shown in the inset maps. Reproduced with permission of the American Geophysical Union.

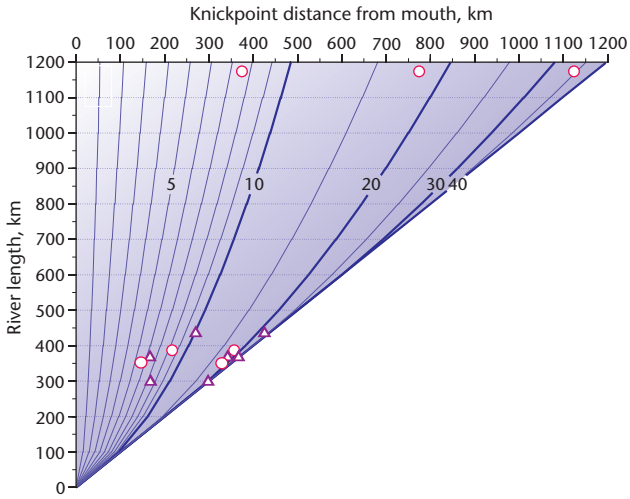

Fig. 5.32 Look-up chart for estimating the timing of uplift events from the position of knickpoints along the river profile. Erosion parameters are advective coefficient $v = 50\,m^{1-m}Myr^{-1}$, exponent for distance $m = 0.5$, and erosional diffusivity $\kappa = 10^5\,m^2\,Myr^{-1}$. Numbered curves are isochrons in Myr, which give the timing of the uplift event for a given knickpoint distance from the river mouth. Shown on look-up chart are three rivers from the Bié dome, southwest Africa (open circles), and three rivers from the South Africa dome (open triangles), each with 2 or 3 knickpoints. From Roberts & White (2010, fig. 15), reproduced with permission of the American Geophysical Union. See also Appendix 47.

region, which experienced uplift over the Yellowstone hotspot, also yielded valuable information on the timing and amount of dynamic topography (Roberts *et al.* 2012).

It is argued that rapid changes in Miocene shoreline positions and a change in flow direction of the paleo-Amazon River took place as a result of surface elevation changes driven by the subduction of oceanic slabs beneath the South American continent (Shephard *et al.* 2010) (Fig. 5.33). The impact of mantle dynamics on drainage network is also seen in the case of the Yellowstone hotspot (Beranek *et al.* 2006; Wegmann *et al.* 2007).

The rate of motion of an overlying plate relative to a mantle flow structure should determine the amplitude, wavelength and longevity of topographic uplift. Let us take two contrasting situations. In the first case of a rapidly moving plate relative to the mantle, such as the northward movement of the Australian plate in the Pliocene to Recent (Heine *et al.* 2010), the uplift is short-lived and relative sea-level changes, recognised by shoreline migration, regionally variable. In the second case of a slowly moving plate relative to the mantle, shoreline migration may be uniform over very large distances, giving the impression of a eustatic control.

5.4.2 Cratonic basins

Among the many hypotheses for the formation of cratonic basins (Allen & Armitage 2012 for summary), a common theme is the thermal contraction of the lithosphere following heating (Sleep & Snell 1976; Xie & Heller 2009). Cratonic basins are described and discussed in relation to lithospheric stretching in §3.2.1. Models of stretching of a continental plate assume that the basal boundary is isothermal (McKenzie 1978a) or experiences a constant heat flow (Kaminski & Jaupart 2000). Instead, the base of the lithosphere can be treated as the boundary between a 'stagnant' or insulating continental lid and a convecting underlying mantle (Sleep 2009). In this case the uplift and subsidence of the Earth's surface constitutes dynamic topography.

Dynamic topography may therefore be manifested on the continents at the present day, apart from the distribution of hotspots and highspots (§5.2.6), in the regions of sag-like subsidence of cratonic basins (Fig. 5.34). The Eyre Basin of Australia (Alley 1998; Veevers *et al.* 1982), the Congo Basin of Africa (Downey & Gurnis 2009) and the Hudson Bay of Canada (Hanne *et al.* 2004) are potentially examples. Some workers have suggested that basins of this type, such as the Congo Basin, are located over downwellings of convective cells in the mantle (Hartley & Allen 1994; Heine *et al.* 2008; Downey & Gurnis 2009). This would explain the lack or paucity of evidence for stretching of the continental crust under some cratonic basins (Allen & Armitage 2012). If cratonic basins are located over downwellings, these convective cells must be attached to the overlying plate, since the locus of subsidence stays fixed relative to the continental crust for protracted periods of time, despite relative motion of plates with respect to the stationary reference frame of the sub-plate mantle. Other workers attribute sag-type subsidence to the ponding of plume material in a closed region beneath the continental plate caused by thinning (Sleep 2009).

The subsidence histories revealed by stratigraphic thicknesses penetrated in boreholes in cratonic basins can be matched by predictions from a range of models, including slow strain rate uniform stretching of an initially thick lithosphere (Armitage & Allen 2010) as well as those invoking dynamic effects transmitted from an underlying convecting mantle.

5.4.3 The history of sea-level change and the flooding of continental interiors

Since the oceanic lithosphere is the cooled thermal boundary layer of the underlying mantle convection system, its root-age trend for ocean bathymetry should play an important role in controlling long-term global sea level through its effect on ocean basin volume. This effect may operate in a number of ways: (i) changes over time in the temperature of the upper mantle beneath the oceanic plates could conceivably result in long-term global sea-level changes. As an illustration of this potential, it is known that the depth of the mid-ocean ridge crests, where unaffected by plumes, varies broadly over a depth range of 1 km. A modest temperature change in the upper mantle of just 40–50 °C would generate this order of variation in seafloor topography. If the thermal structure of the mantle changed significantly over geological time, such changes might be manifested in variations in the extent to which continents are flooded. (ii) Growth in the size of a newly formed ocean basin would cause a temporal increase in the average age of the ocean floor, and therefore an increase in the volume of the ocean basin, with no change in the production rate of new seafloor (Xu *et al.* 2006). This process has been used to explain the Cenozoic sea-level fall as a result of the progressive aging of the world's ocean basins.

If the root-age depth of the ocean floor of the form $d = a + bt^{1/2}$ (where d is seafloor depth, t is age, and a and b are constants), or *thermal topography*, is subtracted from the observed seafloor bathymetry (Davies & Pribac 1993), the mid-ocean ridges are removed, and a broad swell is observed in the central and western Pacific, with a

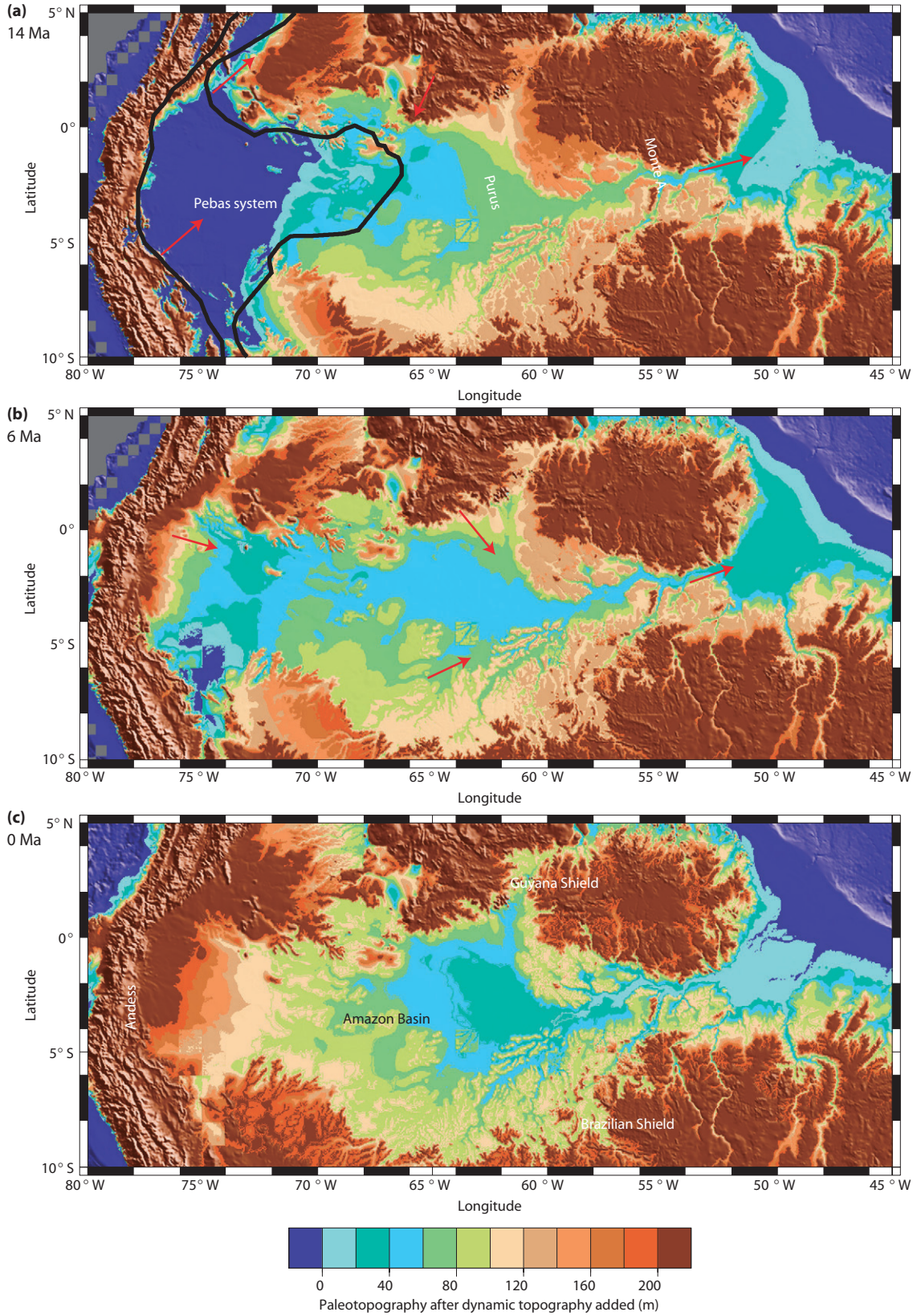

Fig. 5.33 Paleogeography of the Amazon Basin region at 14 Ma (a), 6 Ma (b) and present day (c), showing the reversal of paleodrainage of the Amazon River in the late Miocene. Paleotopographies include calculation of dynamic topography caused by subduction of the Farallon, Phoenix and Nazca plates. Red arrows show sediment transport directions. From Shephard *et al.* (2010). Reprinted by permission from Macmillan Publishers Ltd.

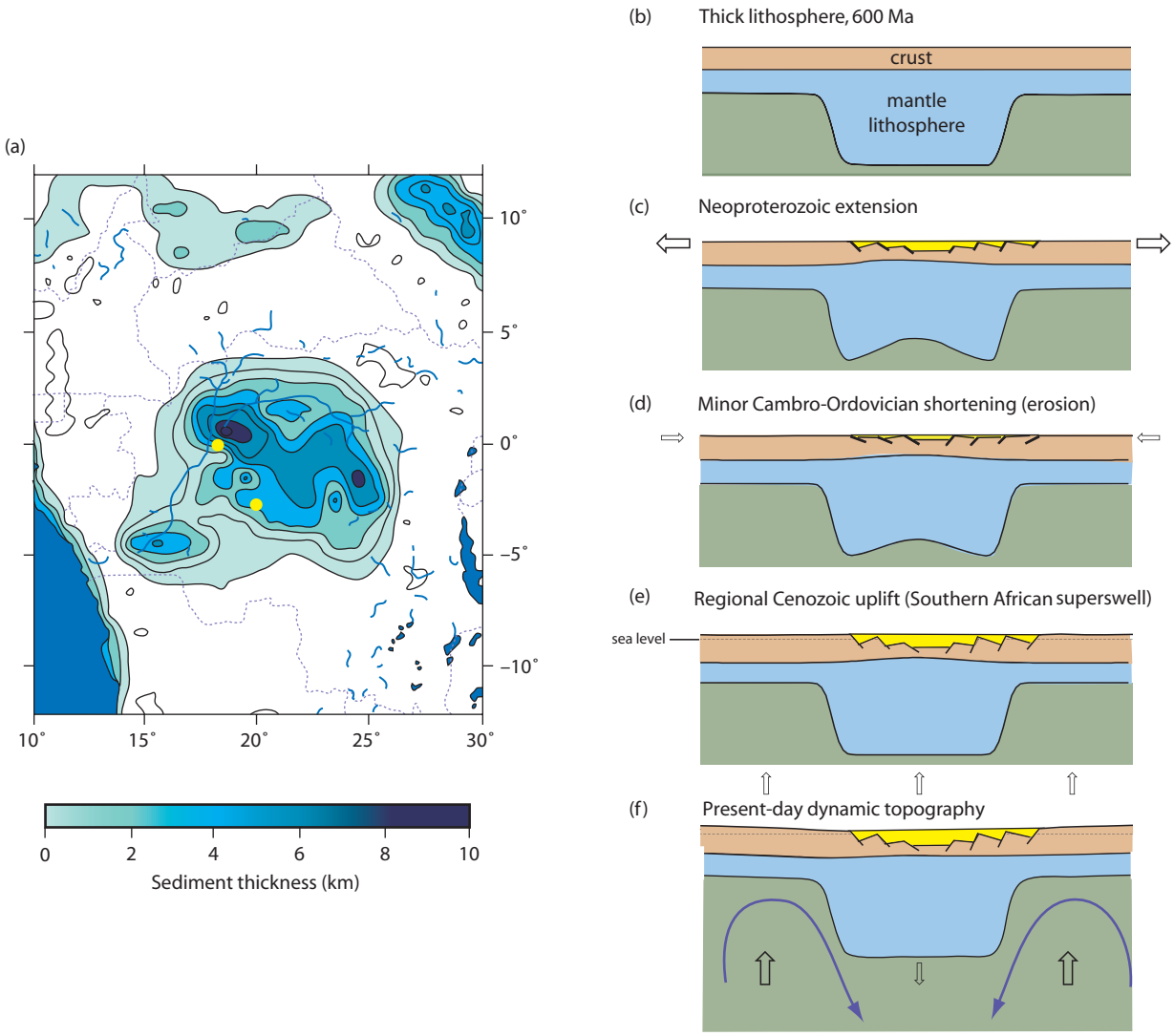

Fig. 5.34 Mantle circulation may be involved in the evolution of some cratonic basins, such as the Congo Basin (after Downey & Gurnis 2009). Convective circulation in the mantle may be responsible for the late Cenozoic to present-day subsidence of the basin and the uplift of the surrounding annulus (Hartley & Allen 1994; Crosby *et al*. 2010; Downey & Gurnis 2009). (a) Sediment isopachs showing roughly circular basin outline with subsidiary depocentres. Yellow circles are borehole locations. (b) to (f) show sequential evolution from Neoproterozoic to present-day. Reproduced with permission of John Wiley & Sons, Inc.

broad low observed between Australia and Antarctica (residual topography, Fig. 5.14). The south Pacific feature, several thousand kilometres in extent and hundreds of metres in elevation, is known as a *superswell* (McNutt & Fischer 1987; McNutt 1998; Adam & Bonneville 2005). Superswells correspond to regions of slow seismic velocities from tomographic studies, and with an anomalously high geoid. These observations suggest that superswells overlie relatively warm mantle. They are regions that have escaped the cooling effects of subduction for long (100–200 Myr) periods of time.

Superswells undoubtedly formed in the past. In the south Pacific region, seafloor updoming in the Cretaceous was accompanied by the eruption of flood basalts (Ontong Java Plateau) due to the spawning of new plumes in the heated region below the superswell (Davies & Pribac 1993) (Fig. 5.35). The importance of this observation is that the uplift of the superswell most likely reduced the volume of the ocean basins and displaced water over the continental shelves, causing the sea-level highs characteristic of this period of Earth history (Bond 1978). Assuming a 5000 km-wide superswell of roughly circular planform shape, with an average bathymetric elevation above the regional bathymetry of 500 m, gives a volume of displaced water of 10×10^6 km^3. Since the area of ocean surface is 360×10^6 km^2, and neglecting isostatic compensation, the global water depth increase is approximately 25–30 m, from the effect of one superswell alone. If the effects of thermal expansion of the Cretaceous ocean is also included, the continents are expected to have been inundated extensively during the Cretaceous, as is confirmed from the transgressive nature of marine stratigraphy of this age (Bond 1976, 1978) (Fig. 8.23).

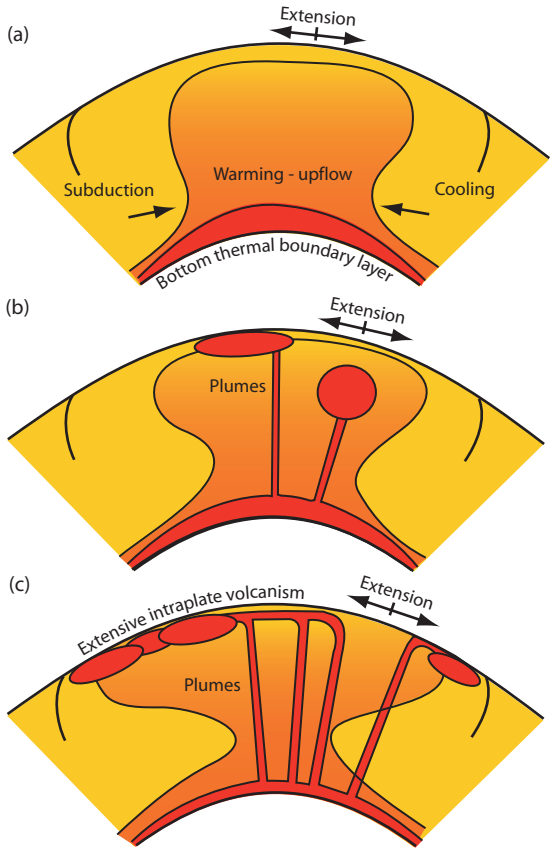

Fig. 5.35 Possible evolution of the Pacific mantle and superswell during the Cretaceous, after Davies & Pribac (1993). In (a) a region of mantle between two subduction zones warms up and causes a thermal doming of the Earth's surface, causing extension. The warming promotes the formation of new plumes that cause igneous accretions to the overlying plate (b). Generations of plumes and their igneous products are formed and transported away through plate motion (c). Note that Davies & Pribac (1993) invoke a large region of mantle heating that spawns plume activity rather than a 'superplume'. Reproduced with permission of the American Geophysical Union.

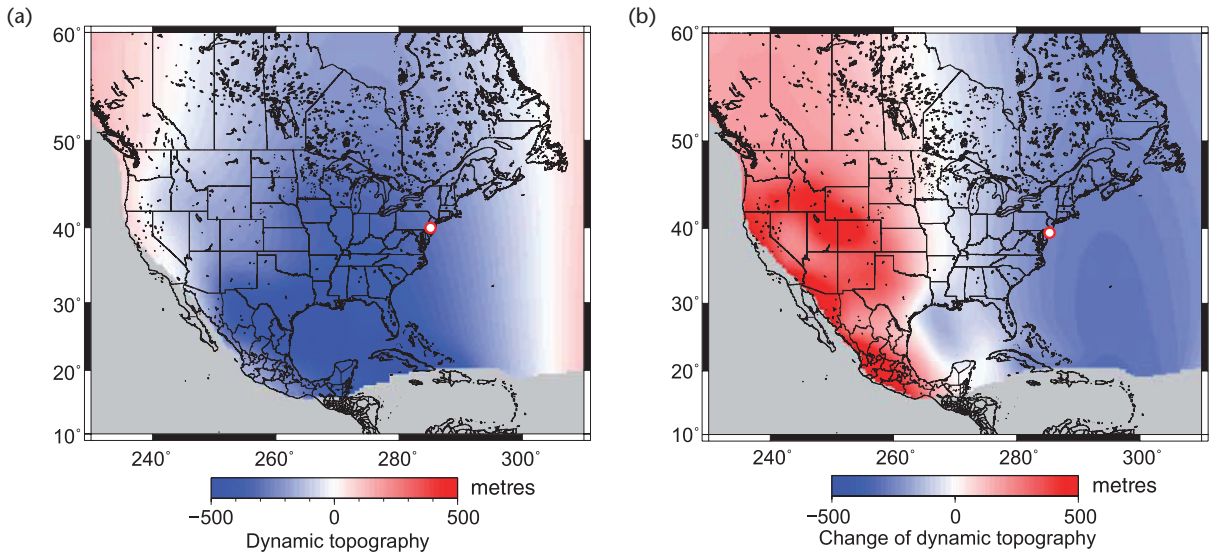

Fig. 5.36 Effect of dynamic topography on estimates of eustatic sea level, after Spasojevic *et al*. (2008). (a) Predicted dynamic topography in North America and the western Atlantic Ocean based on a mantle convection model, with the red circle showing the location of the New Jersey coastal plain. (b) Difference between predicted dynamic topography at 50 Ma (early Eocene) and the present day. The results in (a) and (b) are consistent with the position of paleoshorelines on the coastal plain of eastern USA, and explain some of the discrepancies in Fig. 8.23. Reproduced with permission of the American Geophysical Union.

The long-term trends in global (eustatic) sea level (10–100 Myr duration) and the associated inundations of continental margins are the subject to debate in terms of the methodology used to construct a 'global' cycle chart of sea-level change (Carter 1998; Miall 1992) and in terms of the mechanisms for such long-term trends. With the assumption that these long-term trends are eustatic and therefore globally synchronous (Vail *et al.* 1977a; Haq *et al.* 1987), a mechanism of variation in the spreading rate of mid-ocean ridges is conventionally invoked (Hays & Pitman 1973; Pitman 1978). Doubts have subsequently arisen over whether the history of spreading ridge activity, judged from the age distribution of oceanic crust, matches the known flooding history of continents over the last c.200 Myr (Rowley 2002). In addition, this model neglects the impact of subduction on dynamic topography of adjacent continents (Mitrovica *et al.* 1989; Gurnis 1990b) (see §5.3), which would loosen the connection with spreading rate variations. The continental platforms that have undoubtedly been affected by variations in dynamic topography over geological time are also the source regions for data supporting a global eustatic model.

Convection experiments have been used to predict dynamic topography back through time (Conrad & Gurnis 2003; Moucha *et al.* 2008) (Fig. 5.36). They allow for the cooling effect on the mantle of the descent of cold slabs, such as the Farallon plate (Forte *et al.* 2007), which has resulted in a trend in dynamic topography in the New Jersey area, a region providing critical data for determinations of global sea level in the Cretaceous to present interval (Miller *et al.* 2005). Over the same time interval, there was little relative sea-level change on the conjugate African margin, which was unaffected by the subduction of the Farallon plate, demonstrating that variations in dynamic topography form an important component of the total relative sea-level history of areas providing critical data for the global cycle chart.

In assessing the flooding history of the continents, dynamic topography is likely to modify and even dominate the effects of eustatic change. Variations of 100 m in dynamic topography over periods of tens of millions of years are predicted by spherical shell mantle flow models. By including the effects of dynamic topography, eustatic change cannot be solely due to changes in spreading ridge volumes. Spreading ridge variations, and the attendant long-term geochemical fluxes of the Earth, therefore, do not track eustatic sea level in any simple way.

In summary, from the viewpoint of the basin analyst, one of the most important effects of mantle flow is its impact on sea level and continental inundation.